Supplementary Information (SI) for ChemComm.
This journal is © The Royal Society of Chemistry 2025

Supporting Information

Planar chiral orange-red TADF materials with AIE properties for efficient circularly polarized OLEDs

Xiong Xiao[#], Jia-Qi Liang[#], Jia-Jun Hu, Li Yuan, Jia-Zhen Zhu, Zong-Ju Chen, You Song, Cheng-Hui Li*, You-Xuan Zheng*

State Key Laboratory of Coordination Chemistry, Jiangsu Key Laboratory of Advanced Organic Materials, School of Chemistry and Chemical Engineering, Nanjing University, Nanjing, 210023, P. R. China

E-mail: yxzheng@nju.edu.cn, chli@nju.edu.cn

#X. X. and J.-Q. L. contributed equally to this work.

Table of Contents

1. General information

1.1 Materials and equipment

All reagents and solvents were obtained commercially and used as received. ^{1}H and ^{13}C NMR spectra were recorded on a Bruker ARX 400 spectrometer (400 MHz for ^{1}H and 101 MHz for ^{13}C), using $CDCl_3$ (δ = 7.26 ppm) or CD_2Cl_2 (δ = 5.32 ppm) as solvents and TMS as the internal reference. High-resolution mass spectra (HRMS) were obtained using a Bruker Daltonics MALDI-TOF mass spectrometer. UV–vis absorption spectra were recorded on a Shimadzu UV-2700 spectrophotometer. Photoluminescence (PL) spectra were recorded using a Hitachi F-4600 spectrofluorometer. Low-temperature fluorescence and phosphorescence measurements were carried out on the same instrument after freezing the samples in liquid nitrogen. Absolute photoluminescence efficiencies (Φ_{PL}) were measured using a HORIBA FL3 spectrofluorometer equipped with a calibrated integrating sphere. Thermogravimetric analysis (TGA) was conducted on a Netzsch STA449F3 thermal analyzer under a nitrogen atmosphere at a heating rate of 10 °C min^{-1}.

Single crystals of (*Rac*)-CzCzP, (*R,R*)-tBuCzCzP, and (*S,S*)-tBuCzCzP were grown by vapor diffusion from dichloromethane/methanol solutions. The single-crystal X-ray diffraction data for (*Rac*)-CzCzP were collected using Mo Kα radiation (λ = 0.71073 Å) on a Bruker D8 VENTURE diffractometer with φ and ω scan modes. Data for (*R,R*)-tBuCzCzP and (*S,S*)-tBuCzCzP were acquired using monochromatic Cu Kα radiation (λ = 1.54178 Å) on the same instrument equipped with a PHOTON-100 CMOS detector. These measurements were performed under a nitrogen stream at 223 K using a KRYOFLEX II low-temperature device. Data collection and reduction were carried out using APEX5 V2023.9-2 (Bruker, 2023). Absorption correction was performed using the multi-scan method implemented in SADABS-2016/2 (Bruker, 2016). The crystal structures were solved by direct methods using olex2.solve 1.5 and refined by full-matrix least-squares refinement on F^2 using SHELXL-2018/3 (Sheldrick, 2008) within the Olex2 1.5 interface. Non-hydrogen atoms were refined with anisotropic displacement parameters. Hydrogen atoms were placed in calculated positions and

refined using a riding model (AFIX 23/43/137) with isotropic displacement parameters. In the crystal structure of (*Rac*)-CzCzP, two dichloromethane solvent molecules (C77/C77A and C78/C78A) and their associated chlorine atoms (Cl1/Cl1A, Cl2/Cl2A, Cl3/Cl3A, Cl4/Cl4A) exhibit disorder, modeled with occupancy ratios of 0.850/0.150 and 0.659/0.341, respectively. The disorder was treated using SADI and DFIX restraints (on bond lengths/distances) and SIMU restraints (on displacement parameters). Several carbon atoms in the main molecule (e.g., C1/C1A, C2/C2A) were also modeled with occupancies of 0.659/0.341 and were subjected to appropriate geometric and thermal restraints. Residual electron density arising from the disordered regions was effectively removed through refinement, with the final difference electron density peaks being +0.9639 e/Å³ and −0.7855 e/Å³. In the crystal structure of (*R,R*)-tBuCzCzP, disorder was observed in chlorine atoms (Cl1, Cl2, Cl1A, Cl2A) and carbon atoms (C93, C93A), which were modeled as two components (PART 1 and PART 2) with occupancies of 0.09221 and 0.90779, respectively, controlled by a free variable (FVAR). To maintain equivalent bond lengths (Cl1–C93, Cl1A–C93A, Cl2–C93, Cl2A–C93A), SADI restraints were applied with a standard deviation (σ) of 0.02. SIMU restraints were applied to displacement parameters with σ = 0.02 for general atoms and σ = 0.04 for terminal atoms, within a distance of 2 Å. Additional SADI restraints (σ = 0.01) were imposed to enforce equivalent distances within the C32–C37 ring. DELU restraints (σ = 0.01/0.02) were applied to atoms C32 and C33 to stabilize the refinement. Specific reflections (1 1 1, 3 3 15) were omitted from the refinement. Due to severe disorder, free solvent molecules were not explicitly modeled, and their contributions were excluded from the molecular formula of the unit cell. Detailed crystallographic data are summarized in Table S1. These data can be obtained free of charge from the Cambridge Crystallographic Data Centre via www.ccdc.cam.ac.uk/data_request/cif, using the CCDC numbers 2444969, 2444965, and 2444968.

Cyclic voltammetry (CV) was carried out on a CHI760E electrochemical workstation (Chenhua Instruments) with a polished platinum disk as the working electrode, a platinum wire as the counter electrode, and $Ag/AgNO_3$ (0.1 M in CH_3CN) as the

reference electrode. Tetra-*n*-butylammonium perchlorate (0.1 M) was used as the supporting electrolyte, and the scan rate was set at 0.1 V s^{-1}. Ferrocene/ferrocenium (Fc/Fc^+) served as the internal reference.

The prompt and decay lifetimes of the samples were measured using an FF4 Total time- domain fluorescence lifetime test system. The radiative decay rate constants (k_r) and non-radiative decay rate constants (k_{nr}), intersystem crossing rate constants (k_{ISC}) and reverse intersystem crossing rate constants (k_{RISC}) can be determined by the following equations.[1]

$$k_r = \Phi_p k_p + \Phi_d k_d \approx \Phi_p k_p \quad \text{.....Eq. (1)}$$

$$k_{nr} = \frac{1 - \Phi_{PL}}{\Phi_{PL}} k_r \quad \text{.....Eq. (2)}$$

$$k_{ISC} = k_p - k_r - k_{nr} \quad \text{.....Eq. (3)}$$

$$k_{RISC} = (k_p k_d \Phi_d)/(k_{ISC} \Phi_P) \quad \text{.....Eq. (4)}$$

where k_p and k_d represent the decay rate constants for prompt and delayed fluorescence, respectively, which are dependent on measurements of fluorescence and delayed fluorescence lifetimes (τ_p and τ_d), and analysis of transient and delayed emission components. Φ_p and Φ_d denote the transient and delayed fluorescence components, which can be obtained with the total Φ_{PL} by the transient fluorescence component and delayed fluorescence component share.

1.2 Theoretical calculations method

Density functional theory (DFT) and time-dependent DFT (TD-DFT) calculations were conducted at the B3LYP/6-31G(d,p) level with a PCM solvent model in toluene, using the Gaussian 16 software package.[2] Frontier molecular orbitals (HOMO and LUMO) were visualized using Multiwfn 3.8[3] and VMD.[4] The theoretical calculations performed in the manuscript are for the enantiomers (*S*,*S*)-CzCzP and (*S*,*S*)-tBuCzCzP.

2. Experimental section

2.1 Preparation procedure for 2F-Cz

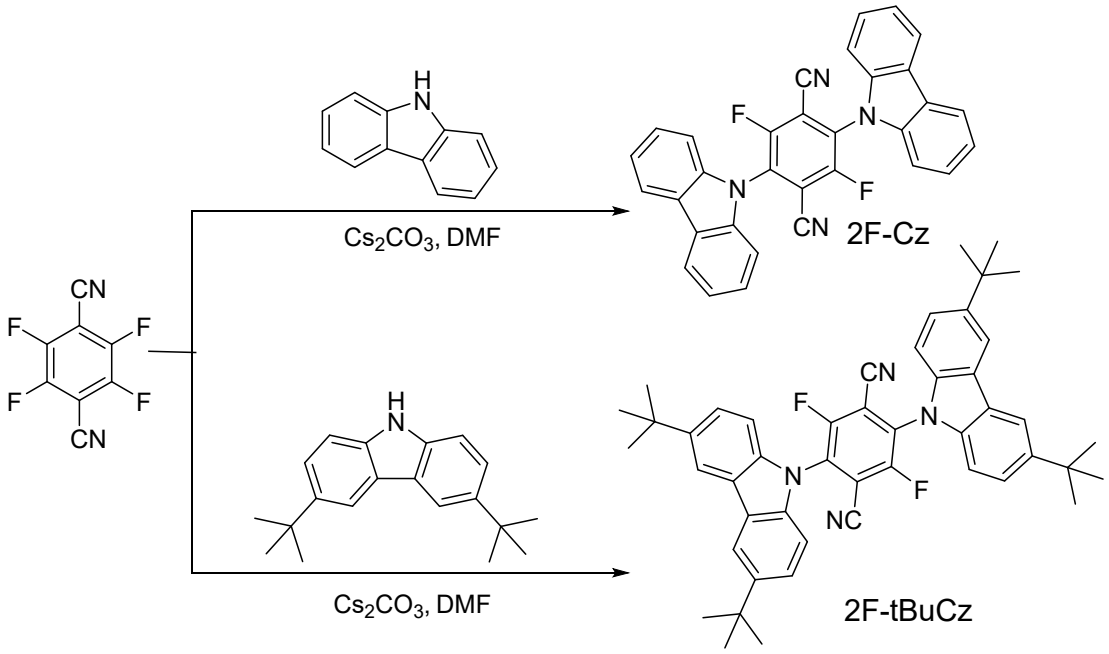

Scheme S1. The synthetic routes of 2F-Cz and 2F-tBuCz.

2,5-Di(9*H*-carbazol-9-yl)-3,6-difluoroterephthalonitrile (2F-Cz): Similar to a previously reported procedure,[5] tetrafluorobenzonitrile (3.00 g, 14.99 mmol, 1 equiv.) and cesium carbonate (9.77 g, 29.98 mmol, 2 equiv.) were dissolved in 30 mL of DMF and stirred until fully dissolved. A pre-sonicated DMF solution (30 mL) of dried carbazole (4.76 g, 28.48 mmol, 1.89 equiv.) was added dropwise at 0 °C. The mixture was stirred at 0 °C for 9 h, then poured into deionized water. The orange-yellow precipitate was collected by filtration and dried. The crude product was dissolved in dichloromethane, sonicated for 1 h, and filtered to remove insoluble residues. The filtrate was concentrated under reduced pressure to yield a crude solid. And the yellow pure 2F-Cz powder (2.36 g, yield: 32%) was recrystallized from acetone

^{1}H NMR (400 MHz, DMSO-d_6) δ 8.34 (dt, *J* = 7.7, 1.0 Hz, 4H), 7.77 (d, *J* = 8.2 Hz, 4H), 7.59 (ddd, *J* = 8.3, 7.2, 1.2 Hz, 4H), 7.45 (ddd, *J* = 8.0, 7.2, 0.9 Hz, 4H). ^{13}C NMR (101 MHz, DMSO) δ 139.93, 127.20, 123.97, 122.41, 121.39, 111.32, 110.46. MALDI-TOF MS: m/z Calcd. for $C_{32}H_{16}F_2N_4$ m/z: 494.13, Found 718.46.

2.2 Preparation procedure for 2F-tBuCz

2,5-Bis(3,6-di-tert-butyl-9H-carbazol-9-yl)-3,6-difluoroterephthalonitrile (2F-tBuCz): Following the same procedure as for 2F-Cz, a DMF solution (30 mL) of dry 3,6-di-tert-butylcarbazole (7.96 g, 28.48 mmol, 1.89 equiv.), prepared by pre-sonication, was added dropwise to the DMF solution of (3.00 g, 14.99 mmol, 1 equiv.) and cesium carbonate (9.77 g, 29.98 mmol, 2 equiv.). After 9 h of stirring at 0 °C, the reaction mixture was poured into deionized water. The crude product was collected by filtration and purified by silica gel column chromatography (300–400 mesh, PE/DCM = 5:1, v/v) to afford orange powder 2F-tBuCz (4.20 g, yield: 39%). ^{1}H NMR (400 MHz, CD_2Cl_2) δ 8.22 (dd, *J* = 2.0, 0.7 Hz, 4H), 7.60 (dd, *J* = 8.6, 1.9 Hz, 4H), 7.23 (dd, *J* = 8.7, 1.0 Hz, 4H), 1.48 (s, 36 H). ^{13}C NMR (101 MHz, CD_2Cl_2) δ 155.20, 145.59, 137.90, 124.62, 124.40, 117.22, 109.26, 53.96, 53.69, 53.42, 53.15, 52.88, 34.82, 31.62. MALDI-TOF MS: m/z Calcd. for $C_{48}H_{48}F_2N_4$ m/z: 718.38, Found 718.46.

2.3 Synthesis of CzCzP

[2]Paracyclo[2](1,4)carbazolophane (carbazolophane, CzCzP): The carbazolophane (CzP) was prepared according to the previous article.[6]

2,5-Di(19*H*-1(1,4)-carbazola-4(1,4)-benzenacyclohexaphane-19-yl)-3,6-di(9*H*-carbazol-9-yl)terephthalonitrile (CzCzP): To a 100 mL two-necked flask, 0.14 g (0.483 mmol, 2.05 equiv.) of dried CzP and 0.08 g (0.714 mmol, 3 equiv.) of potassium tert-butoxide (tBuOK) were added, and dissolved in 10 mL of DMF. The mixture was heated at 60 °C under a nitrogen atmosphere for 30 min. Subsequently, 10 mL of a DMF solution containing 0.12 g (0.238 mmol, 1 equiv.) of 2F-Cz was added to the mixture, and the reaction proceeded at 115 °C for 24 h. Upon completion, the reaction mixture was poured into water, and the resulting precipitate was filtered to yield the crude product. After purification via silica gel column chromatography (eluent: PE/DCM = 1:1) (0.10 g, yield: 41.4 %) of orange-red solid powder was isolated.

(*R,R*)-CzCzP：The enantiomer (*R,R*)-CzCzP (0.07 g, yield: 58.3%) was obtained following the same procedure, using (*R*)-CzP (0.068 g, 0.228 mmol, 2.05 equiv.), ^{t}BuOK (0.04 g, 0.333 mmol, 3 equiv.), and 2F-Cz (0.06 g, 0.111 mmol, 1 equiv.) as starting

materials.

(*S,S*)-CzCzP：The pure enantiomer (*S,S*)-CzCzP (0.06 g, yield: 49.8%) was obtained using the same procedure, with (*S*)-CzP (0.07 g, 0.236 mmol, 2.05 equiv.), ^{t}BuOK (0.04 g, 0.346 mmol, 3 equiv.), and 2F-Cz (0.06 g, 0.115 mmol, 1 equiv.) as starting materials. ^{1}H NMR (400 MHz, $CDCl_3$) δ 7.68 (dd, *J* = 7.8, 4.0 Hz, 4H), 7.57 – 7.38 (m, 10H), 7.32 (dq, *J* = 7.9, 4.7, 2.6 Hz, 2H), 7.24 (t, *J* = 7.3 Hz, 2H), 6.83 (t, *J* = 7.5 Hz, 2H), 6.37 (dt, *J* = 22.4, 7.4 Hz, 6H), 6.24 (d, *J* = 7.7 Hz, 2H), 6.07 (t, *J* = 8.5 Hz, 4H), 5.54 (dd, *J* = 45.1, 7.8 Hz, 4H), 3.57 (dd, *J* = 13.0, 9.2 Hz, 2H), 3.13 (dd, *J* = 9.7, 4.9 Hz, 4H), 3.06 – 2.59 (m, 10H). ^{13}C NMR (101 MHz, $CDCl_3$) δ 143.01, 139.59, 138.93, 138.90, 138.09, 137.90, 137.28, 134.73, 132.05, 131.90, 131.71, 129.75, 127.71, 127.60, 127.16, 126.94, 125.55, 125.51, 124.43, 124.31, 123.87, 123.22, 122.62, 122.46, 121.46, 121.12, 120.81, 120.68, 119.57, 113.48, 110.37, 109.45, 109.25, 77.36, 77.04, 76.72, 34.30, 33.70, 33.25, 32.81. MALDI-TOF MS: m/z Calcd. for $C_{76}H_{53}N_6^+$ $[M+H]^+$: 1049.43, Found 1049.65.

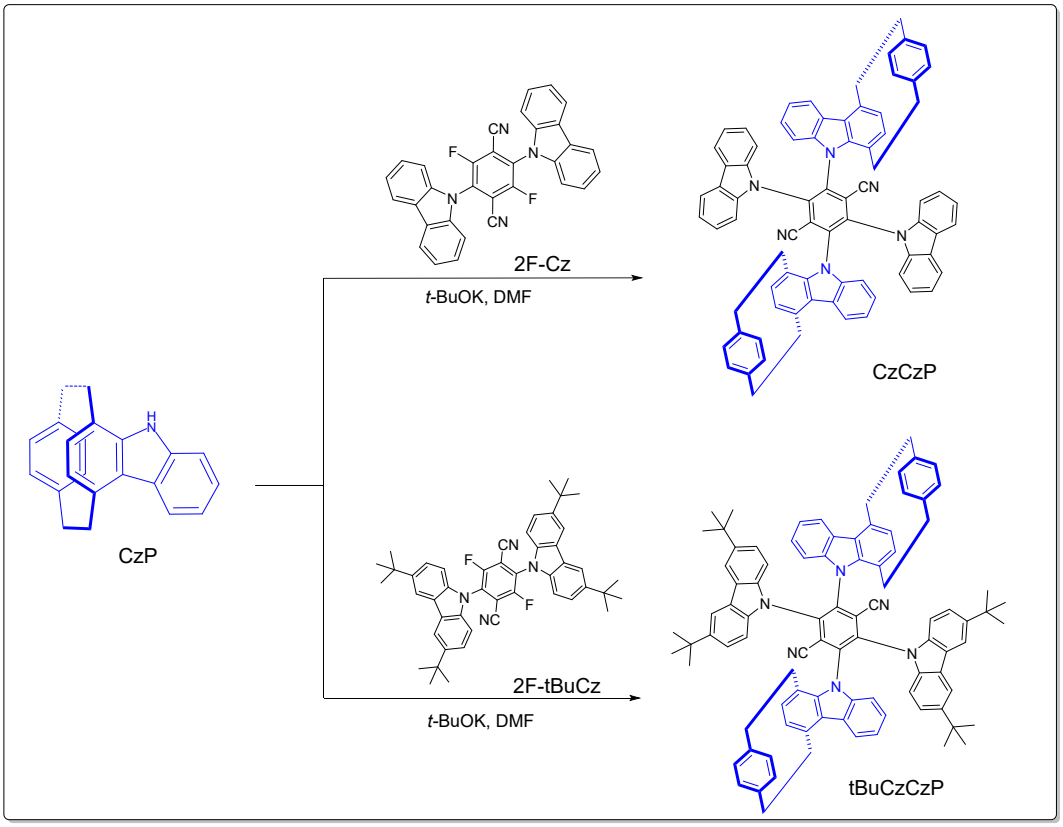

Scheme S2. The synthetic routes of CzCzp and tBuCzCzP.

2.4 Synthesis of tBuCzCzP

2,5-Di(19*H*-1(1,4)-carbazola-4(1,4)-benzenacyclohexaphane-19-yl)-3,6-bis(3,6-di-*tert*-butyl-9*H*-carbazol-9-yl)terephthalonitrile (tBuCzCzP): In a similar procedure to the synthesis of CzCzP, 0.09 g (0.287 mmol, 2.05 equiv.) of dried CzP and 0.05 g (0.420 mmol, 3 equiv.) of potassium tert-butoxide were initially dissolved in 10 mL of DMF. The mixture was maintained at 60 °C for 30 minutes under a nitrogen atmosphere, and then 10 mL of a DMF solution containing 0.10 g (0.140 mmol, 1 equiv.) of 2F-tBuCz was added. After 24 hours of reaction at 115 °C, the crude product was obtained by pouring the reaction mixture into water and filtering the resulting precipitate. The product, an orange-red solid powder (0.09 g, yield: 50.8%), was purified using silica gel column chromatography (eluent: PE/DCM = 2:1).

(*R,R*)-tBuCzCzP：Following an identical synthetic protocol, (*R,R*)-tBuCzCzP (0.08 g, yield: 55.6 %) was prepared using (*R*)-CzP (0.07 g, 0.232 mmol, 2.05 equiv.), tBuOK (0.04 g, 0.339 mmol, 3 equiv.), and 2F-tBuCz (0.08 g, 0.113 mmol, 1 equiv.) in place of the corresponding reagents.

(*S,S*)-tBuCzCzP：Following an identical synthetic protocol, pure enantiomer (*S,S*)-tBuCzCzP (0.09 g, 61.6% yield) was obtained by employing (*S*)-CzP (0.07 g, 0.236 mmol, 2.05 equiv.), tBuOK (0.04 g, 0.346 mmol, 3 equiv.), and 2F-tBuCz (0.08 g, 0.115 mmol, 1 equiv.) as starting materials.

^{1}H NMR (400 MHz, $CDCl_3$) δ 7.77 – 7.57 (m, 4H), 7.57 – 7.39 (m, 8H), 7.31 (d, *J* = 8.5 Hz, 4H), 6.33 (td, *J* = 37.7, 36.8, 7.9 Hz, 8H), 6.01 (dd, *J* = 26.0, 8.1 Hz, 4H), 5.47 (t, *J* = 6.9 Hz, 4H), 3.69 – 3.44 (m, 2H), 3.12 (t, *J* = 7.2 Hz, 4H), 3.07 – 2.71 (m, 8H), 2.59 (dt, *J* = 15.6, 8.3 Hz, 2H), 1.49 (s, 18H), 1.28 (s, 18H). ^{13}C NMR (101 MHz, $CDCl_3$) δ 144.45, 143.75, 142.45, 139.99, 139.71, 138.77, 137.92, 137.61, 137.39, 136.40, 134.31, 131.83, 131.74, 131.67, 129.49, 127.67, 127.55, 127.20, 126.98, 125.40, 124.70, 124.09, 123.22, 123.00, 122.59, 122.17, 121.59, 121.05, 116.97, 115.46, 113.79, 110.42, 109.19, 108.65, 77.35, 77.03, 76.72, 34.80, 34.38, 34.27, 33.60, 33.17, 32.67, 32.10, 31.79. MALDI-TOF MS: m/z Calcd. for $C_{92}H_{84}N_6Na^+$ $[M+Na]^+$: 1296.67, Found 1296.39.

3 NMR spectra and MALDI-TOF mass spectra

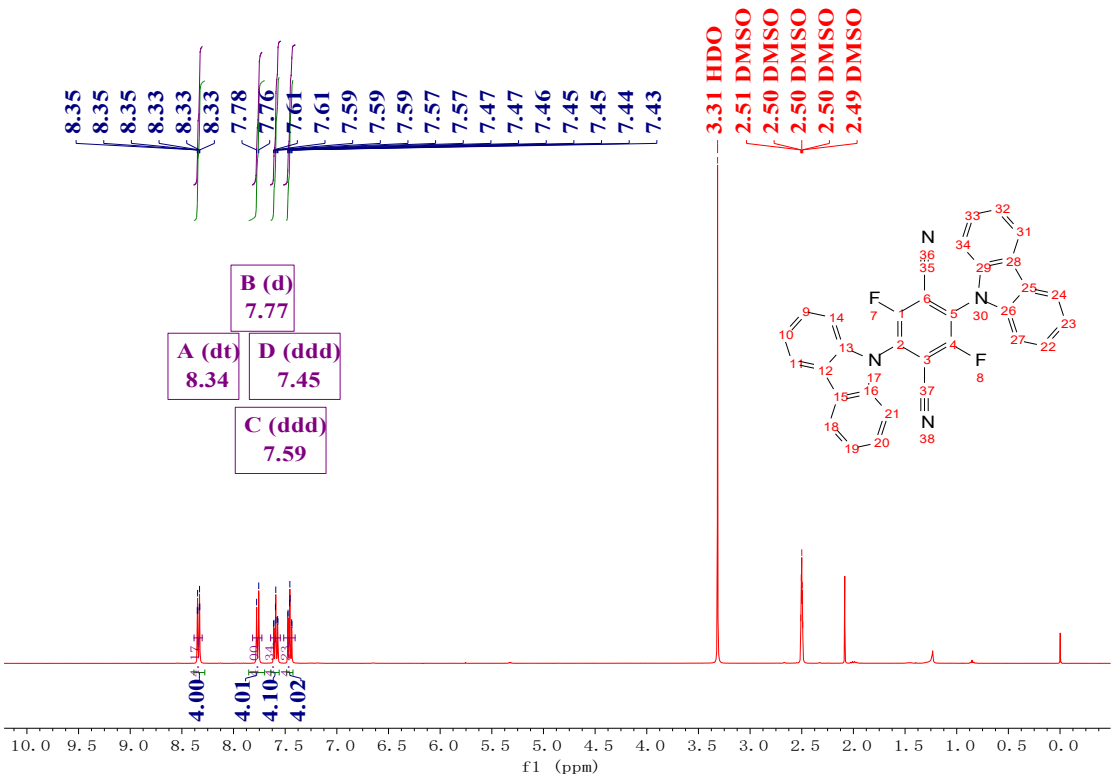

Fig. S1 The ^{1}H NMR spectrum of 2F-Cz in DMSO-d_6 (400 MHz, 298 K).

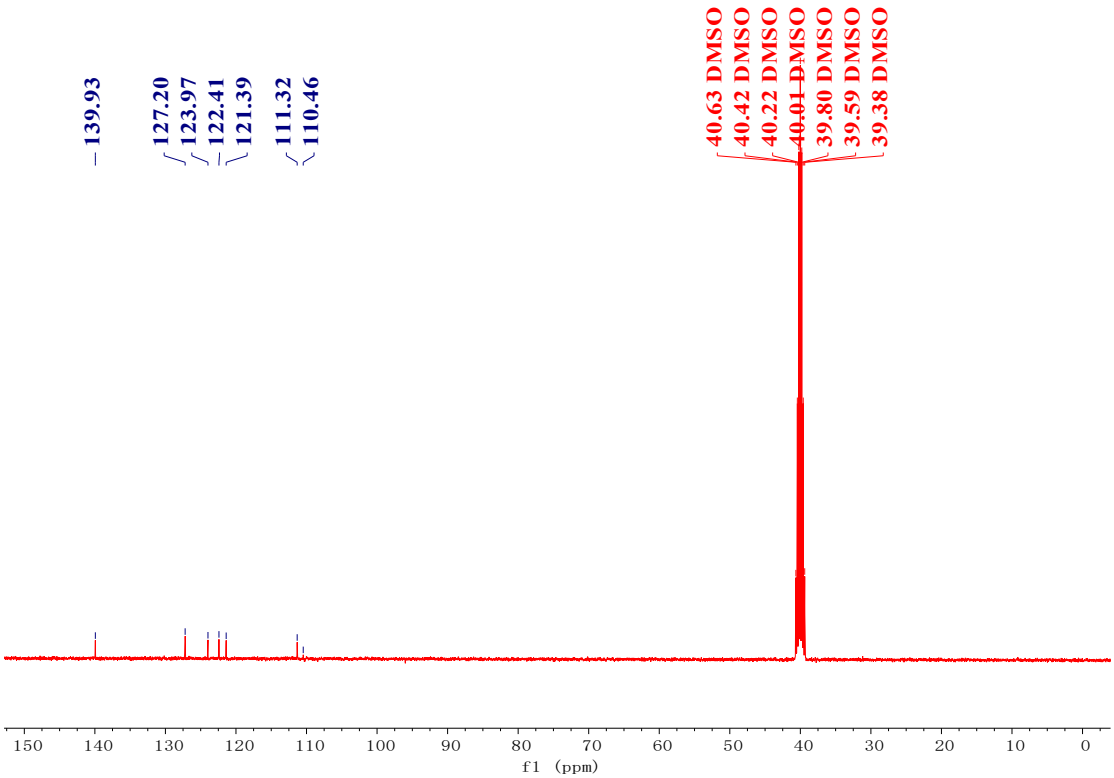

Fig. S2 The ^{13}C NMR spectrum of 2F-Cz in DMSO-d_6 (101 MHz, 298 K).

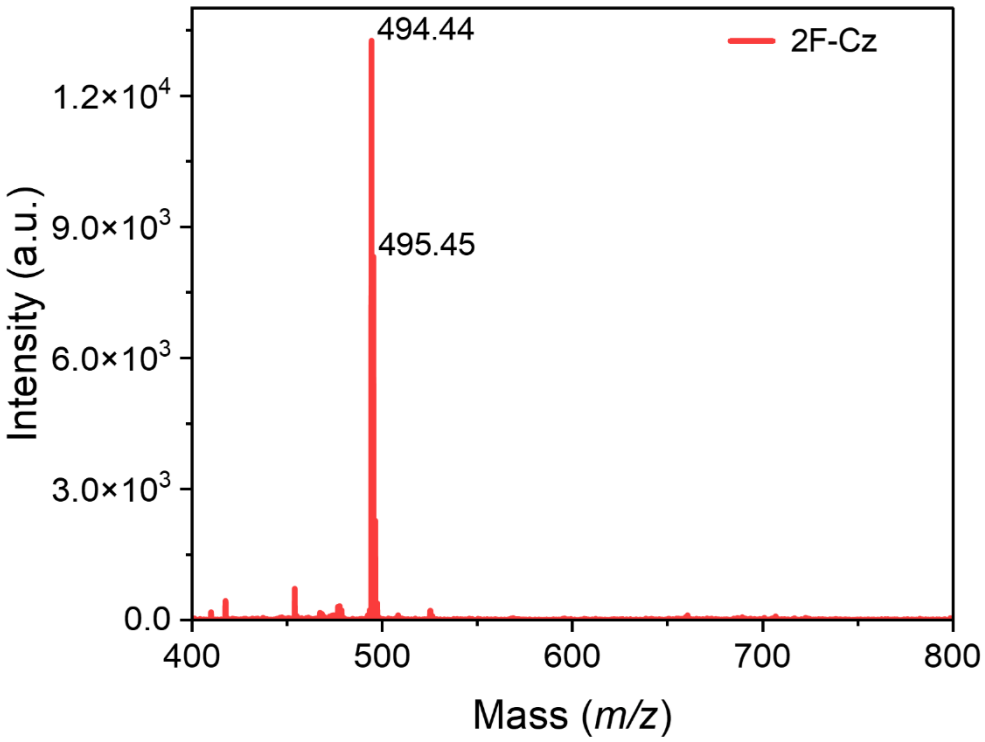

Fig. S3 The MALDI-TOF mass spectrum of 2F-Cz.

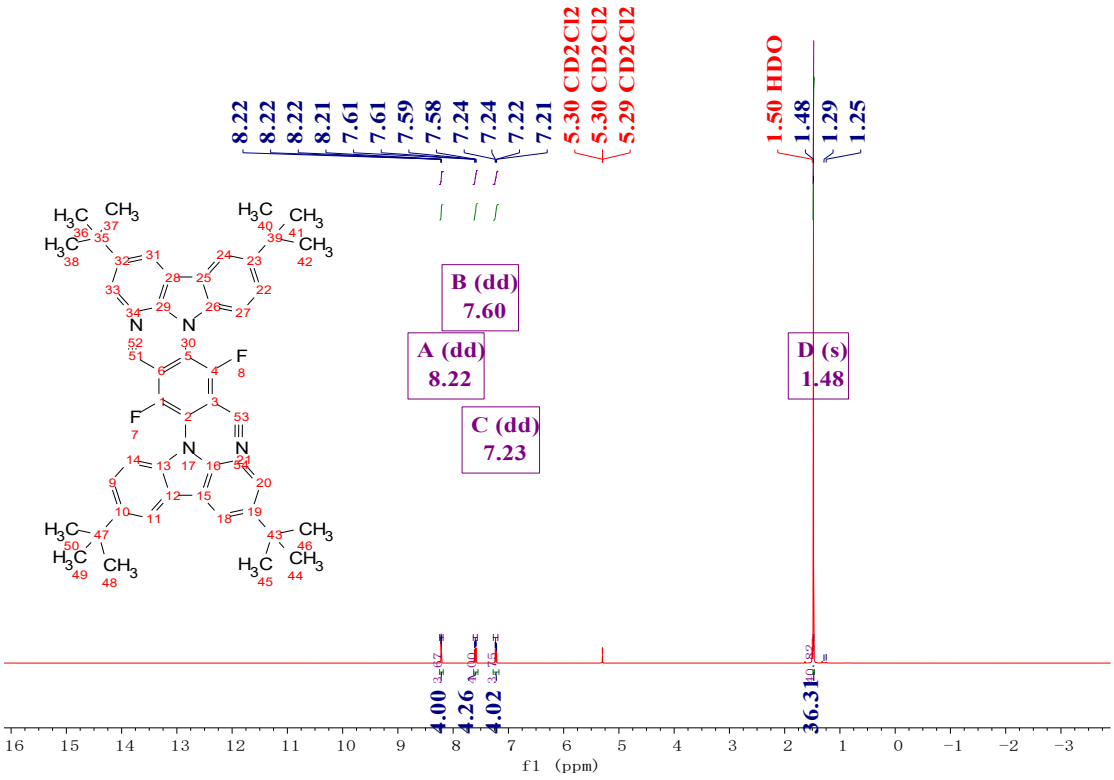

Fig. S4 The ^{1}H NMR spectrum of 2F-tBuCz in CD_2Cl_2 (400 MHz, 298 K).

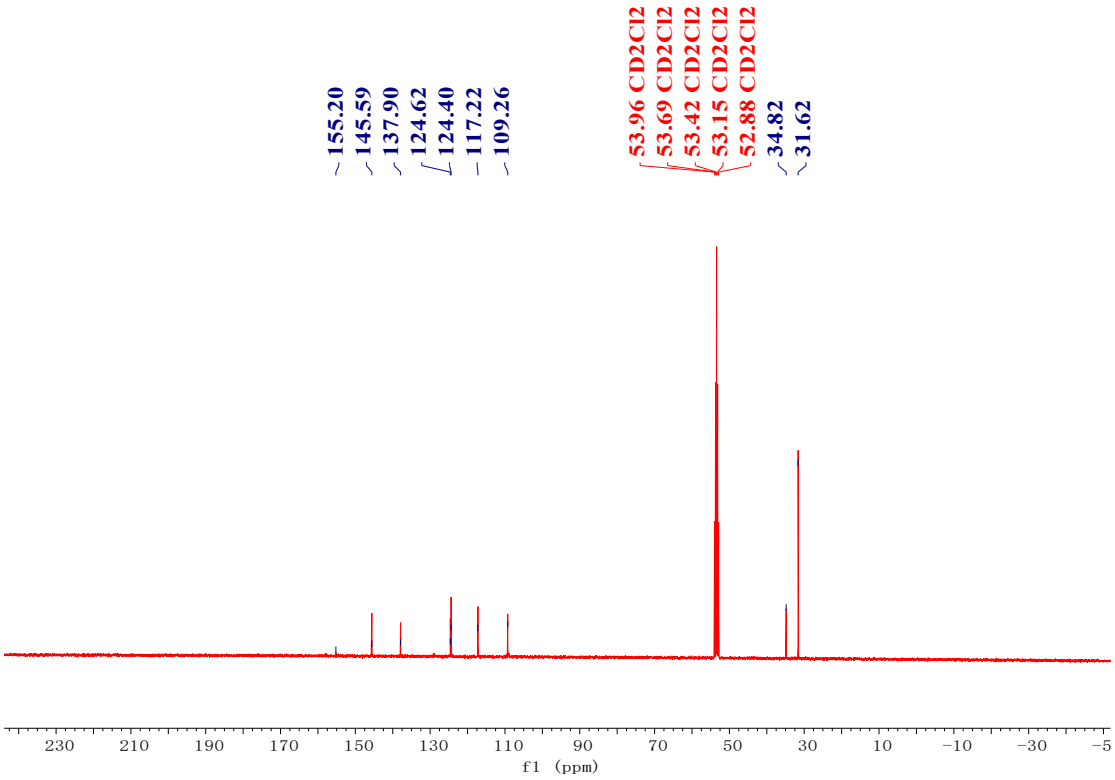

Fig. S5 The ^{13}CNMR spectrum of 2F-tBuCz in CD_2Cl_2 (101 MHz, 298 K).

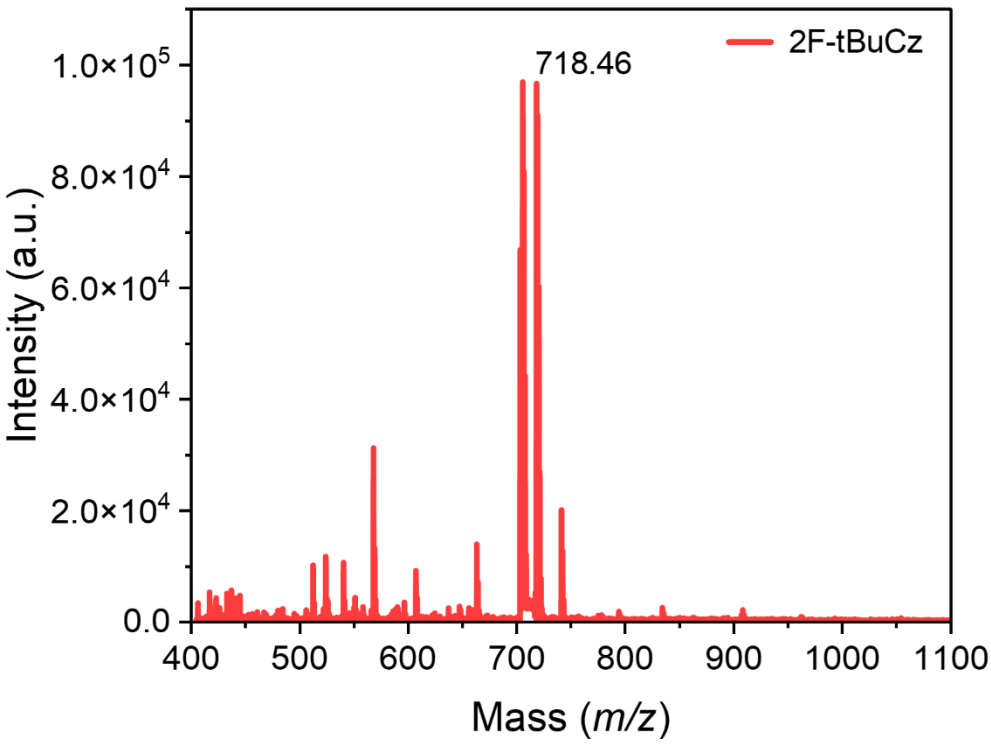

Fig. S6 The MALDI-TOF mass spectrum of 2F-tBuCz.

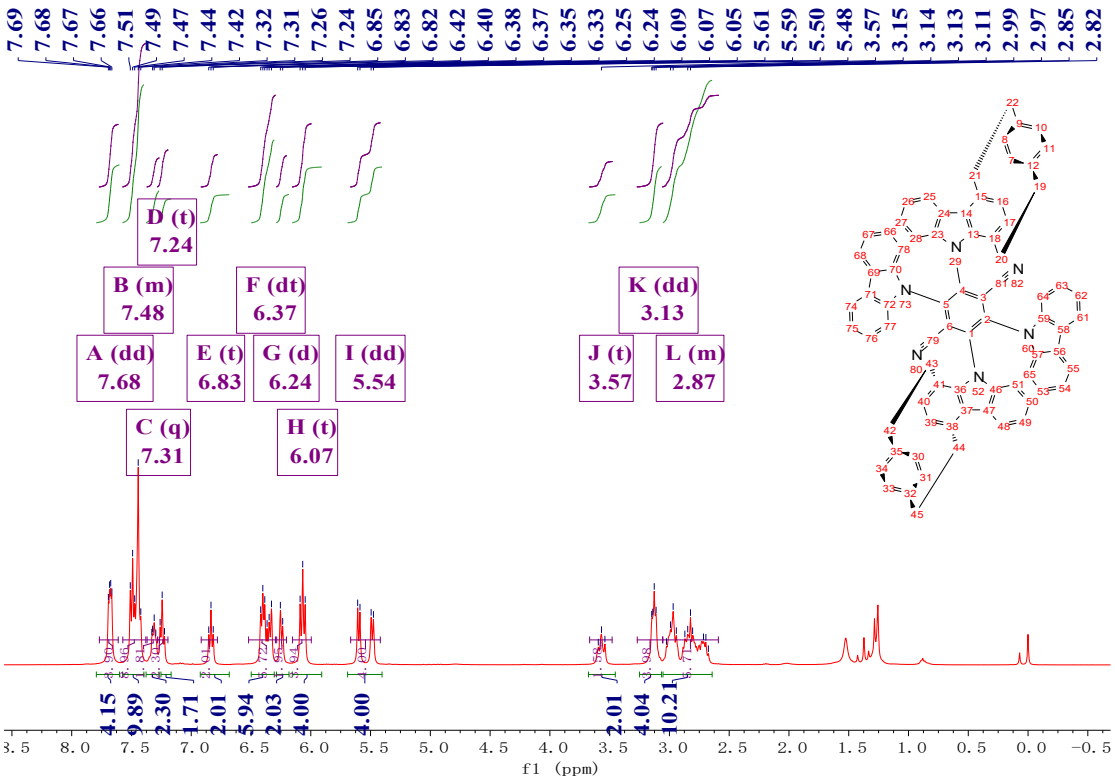

Fig. S7 The ^{1}H NMR spectrum of CzCzP in $CDCl_3$ (400 MHz, 298 K).

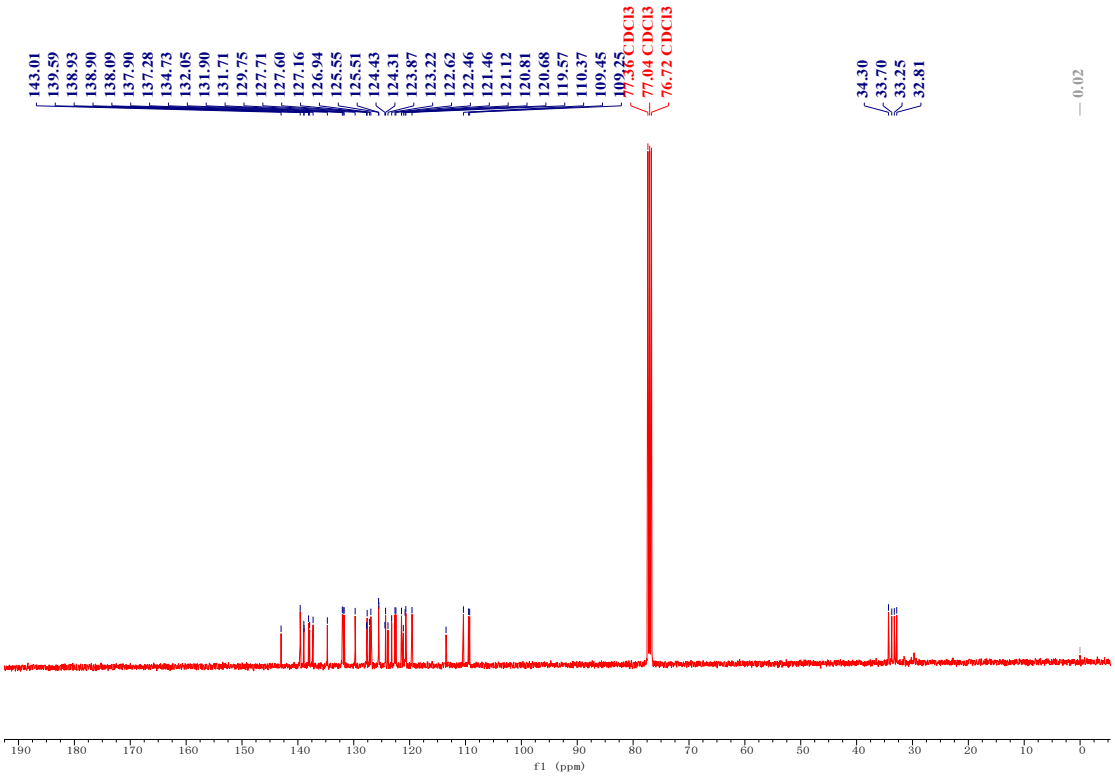

Fig. S8 The ^{13}C NMR spectrum of CzCzP in $CDCl_3$ (101 MHz, 298 K).

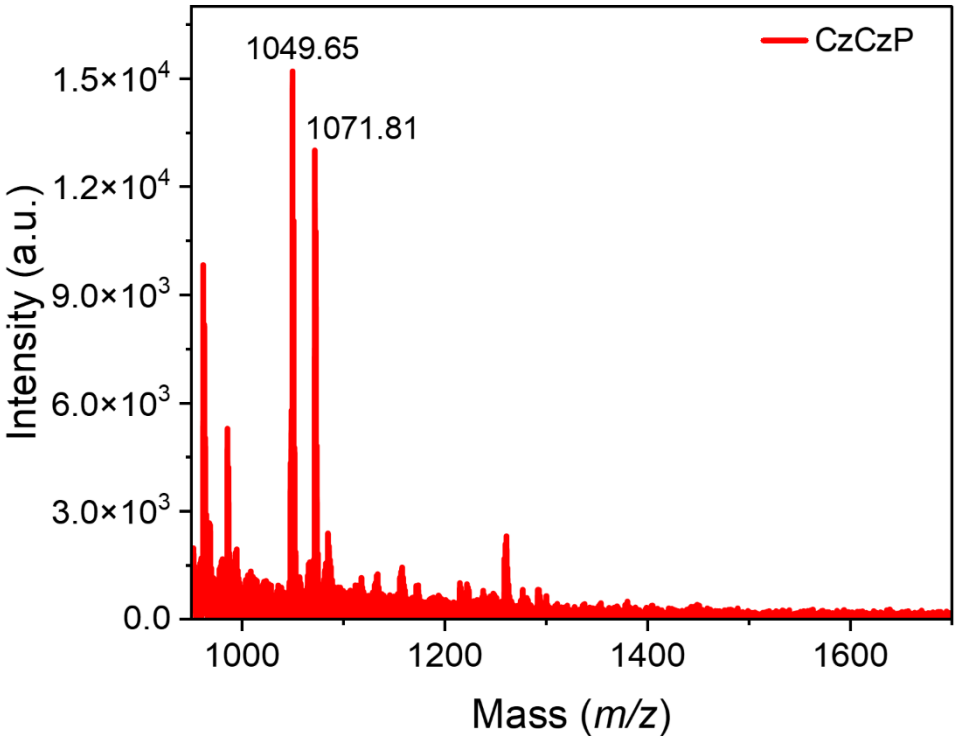

Fig. S9 The MALDI-TOF mass spectrum of CzCzP.

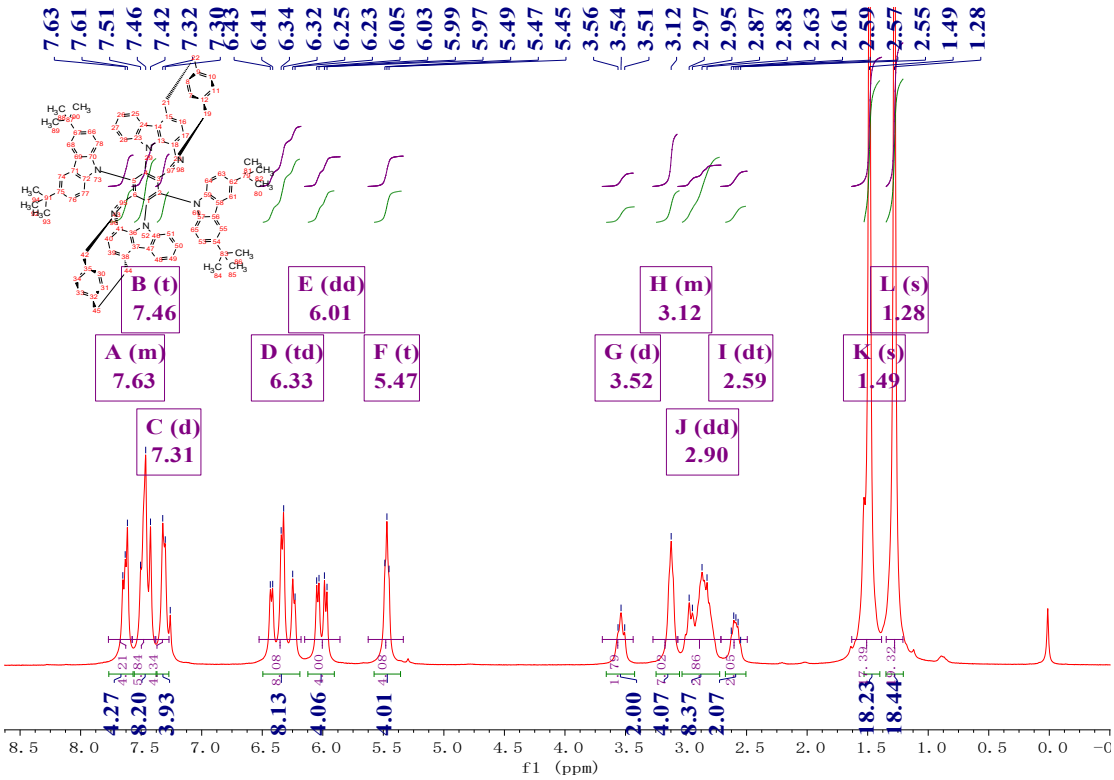

Fig. S10 The ^{1}HNMR spectrum of tBuCzCzP in $CDCl_3$ (400 MHz, 298 K).

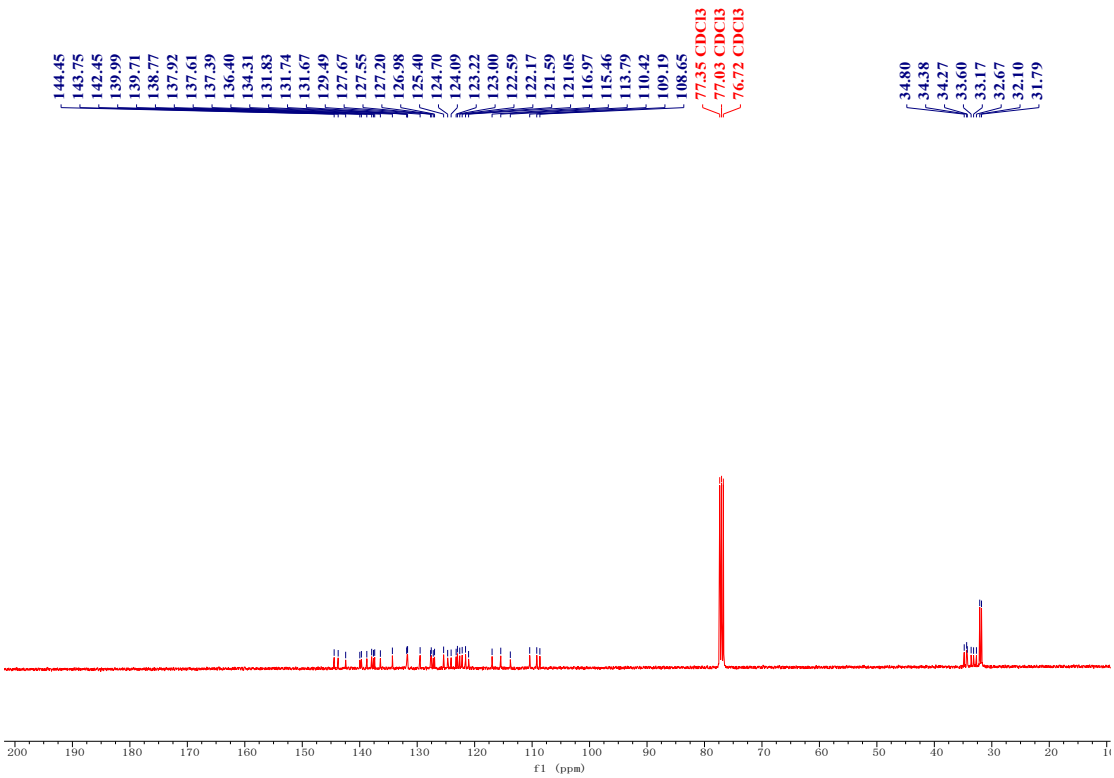

Fig. **S11** The ^{13}CNMR spectrum of tBuCzCzP in $CDCl_3$ (101 MHz, 298 K).

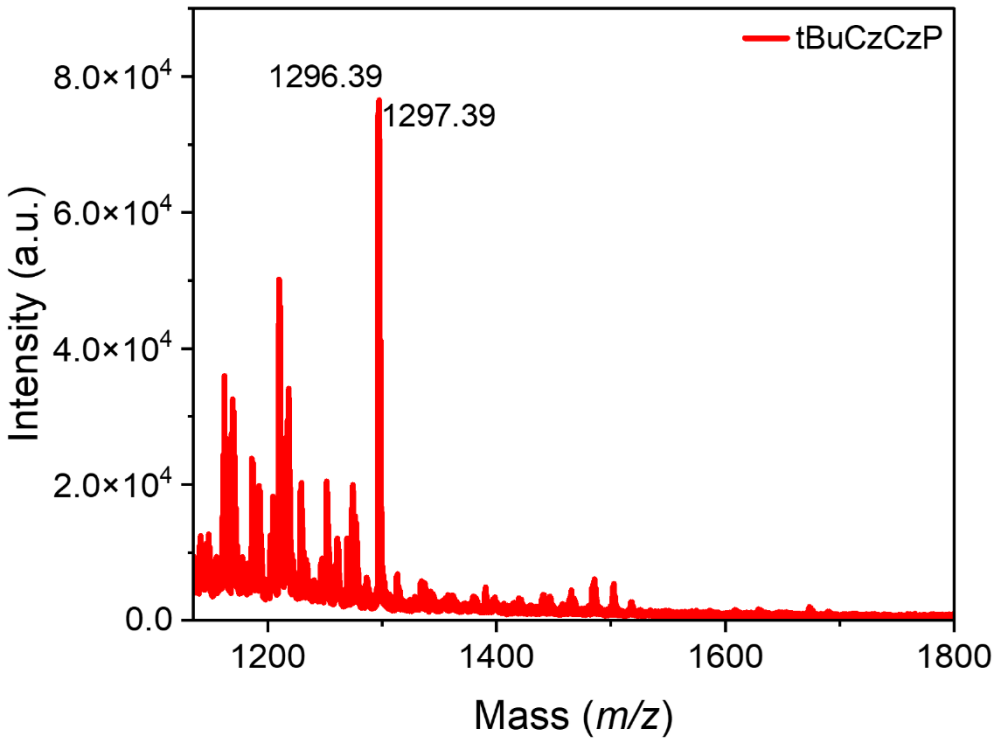

Fig. S12 The MALDI-TOF mass spectrum of tBuCzCzP.

4. HPLC data

HPLC Analysis Conditions: a) Column: Chiralpak IG-3 (50 × 4.6 mm LD，3 μm); b) Mobile phase: Phase A for CO2, and Phase B for IPA (0.05% DEA); c) Gradient elution: IPA (containing 0.05% DEA) in CO_2 from 20% to 60%; d) Flow rate: 3.0 mL min^{-1}.

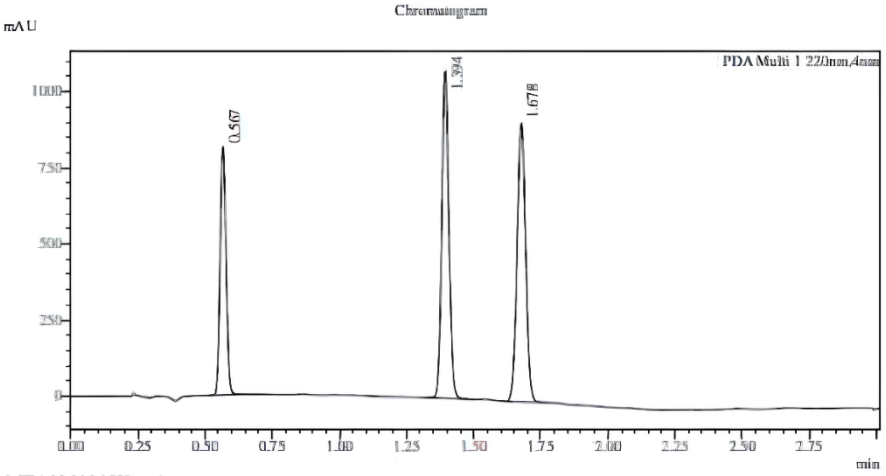

Integration Result

Peak Table

PDA Ch1 220nm

Peak#	Ret. Time	Height	Height%	Resolution(USP)	Area	Area%
1	0.567	795674	29.242	–	1253854	23.787
2	1.394	1018662	37.437	16.882	1985888	37.675
3	1.678	906644	33.321	4.928	2031336	38.537

Fig. S13 HPLC profile of racemic CzP.

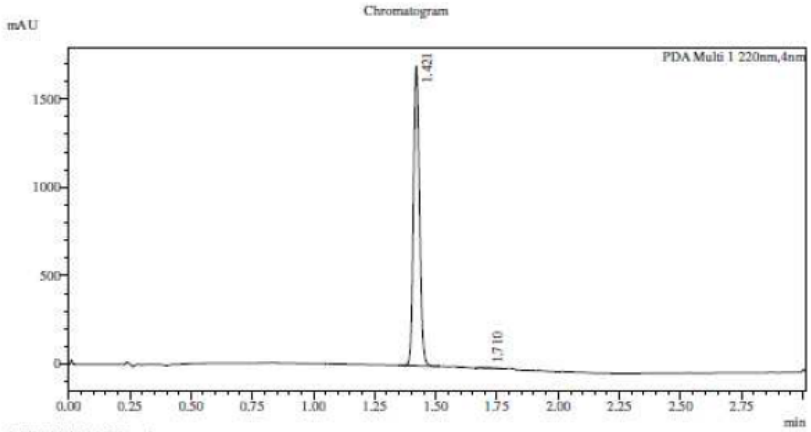

Integration Result

Peak Table

PDA Ch1 220nm

Peak#	Ret. Time	Height	Height%	Resolution(USP)	Area	Area%
1	1.421	1665857	99.734	–	2906278	99.533
2	1.710	4444	0.266	4.038	13630	0.467

Fig. S14 HPLC profile of *S*-CzP.

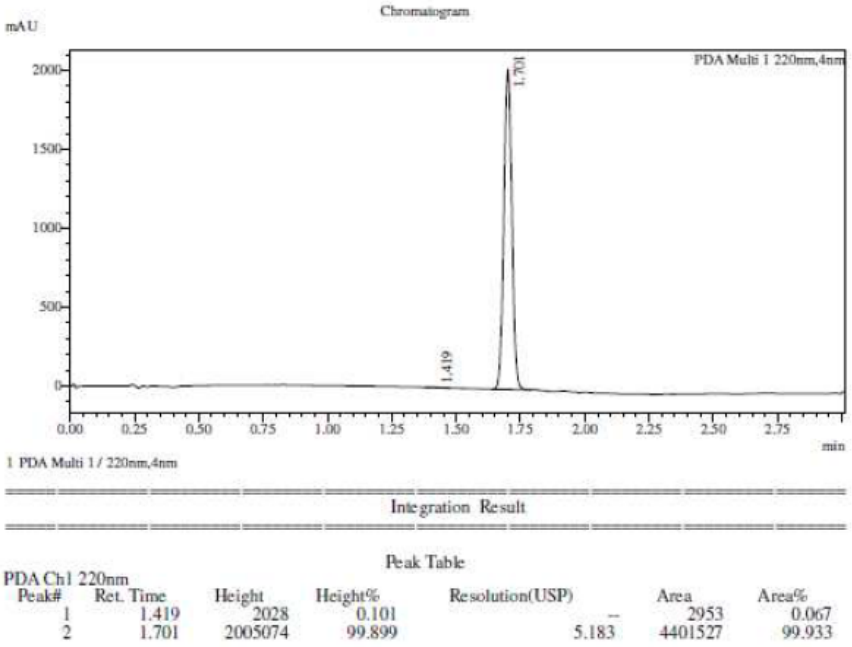

Fig. S15 HPLC profile of *R*-CzP.

5. Thermal stabilities and cyclic voltammetry characteristics

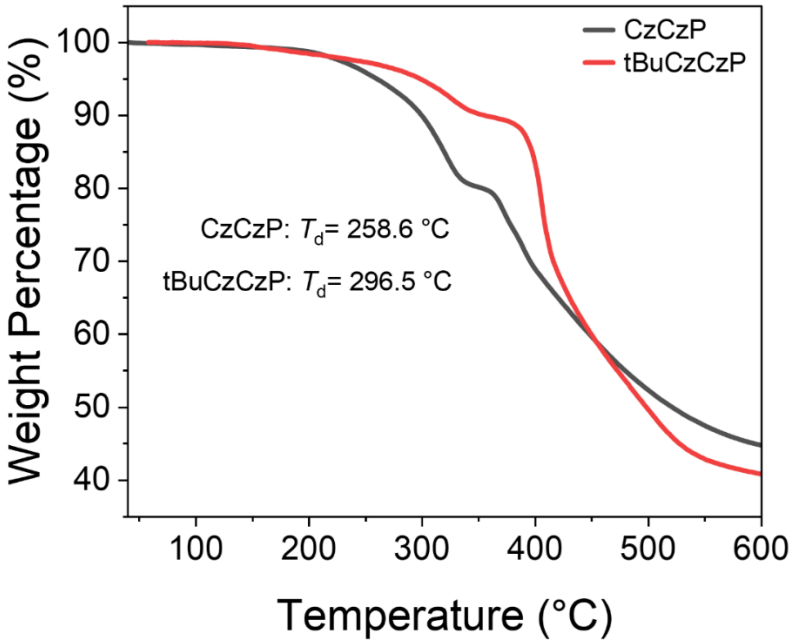

Fig. S16 TGA curves of the two CP-TADF materials.

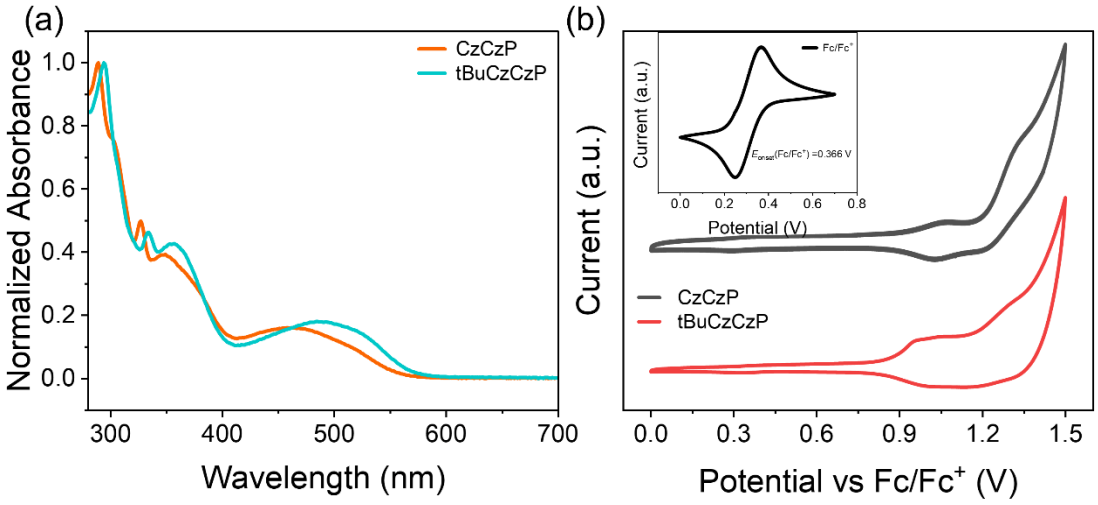

Fig. S17 (a) The UV–vis absorption spectra of CzCzP and tBuCzCzP in CH_3CN (r.t) (b) Cyclic voltammetry curves of CzCzP and tBuCzCzP, measured in CH_3CN containing 0.1 M *tetra*-n-butylammonium hexafluorophosphate. Inset: Cyclic voltammetry diagram ferrocene as the internal standard, and the $E_{(Fc/Fc+)}$ is measured as 0.366 eV.

Table S1. Electrochemical properties of the three emitters.

Emitter	λ_{abs}	E_g^{opt}	E_{onset}(ox)	E_{onset}(Fc^+/Fc)	E_{HOMO} (eV)	E_{LUMO} (eV)
CzCzP	605	2.05	1.04	0.366	-5.48	-3.43
tBuCzCzP	596	2.08	0.96	0.366	-5.40	-3.31

a) Optical gap ($1240/\lambda_{onset}$) according to the onset of UV-vis absorption wavelength obtained from dilute CH_3CN (1×10^{-5} M). b) The onset of oxidation curve measured in CH_3CN containing 0.1 M *tetra*-n-butylammonium hexafluorophosphate. c) $E_{HOMO} = -[E_{ox} - E_{(Fc/Fc+)} + 4.8]$ eV, $E_{(Fc/Fc+)} = 0.0722$ eV. d) $E_{LUMO} = (E_{HOMO} + E_{g,opt})$.[7]

6. X-ray crystallographic data and analysis

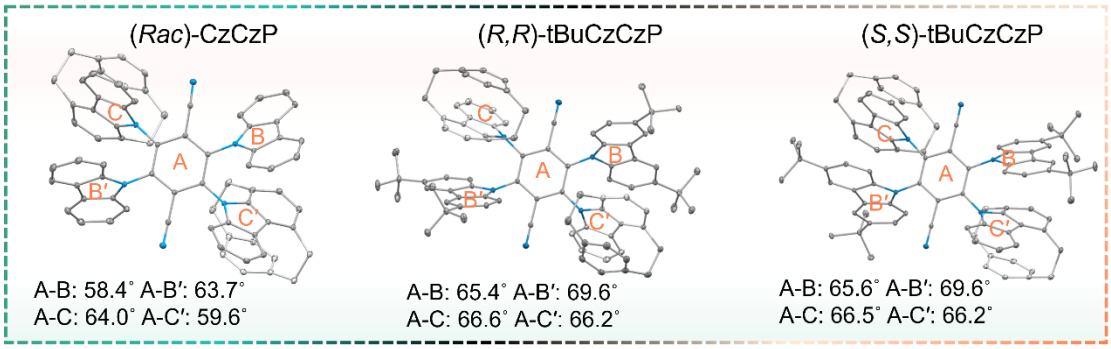

Fig. S18 Single-crystal structures of (*Rac*)-CzCzP and (*R,R*)/(*S,S*)-tBuCzCzP, highlighting dihedral angles between Cz and CzP moieties.

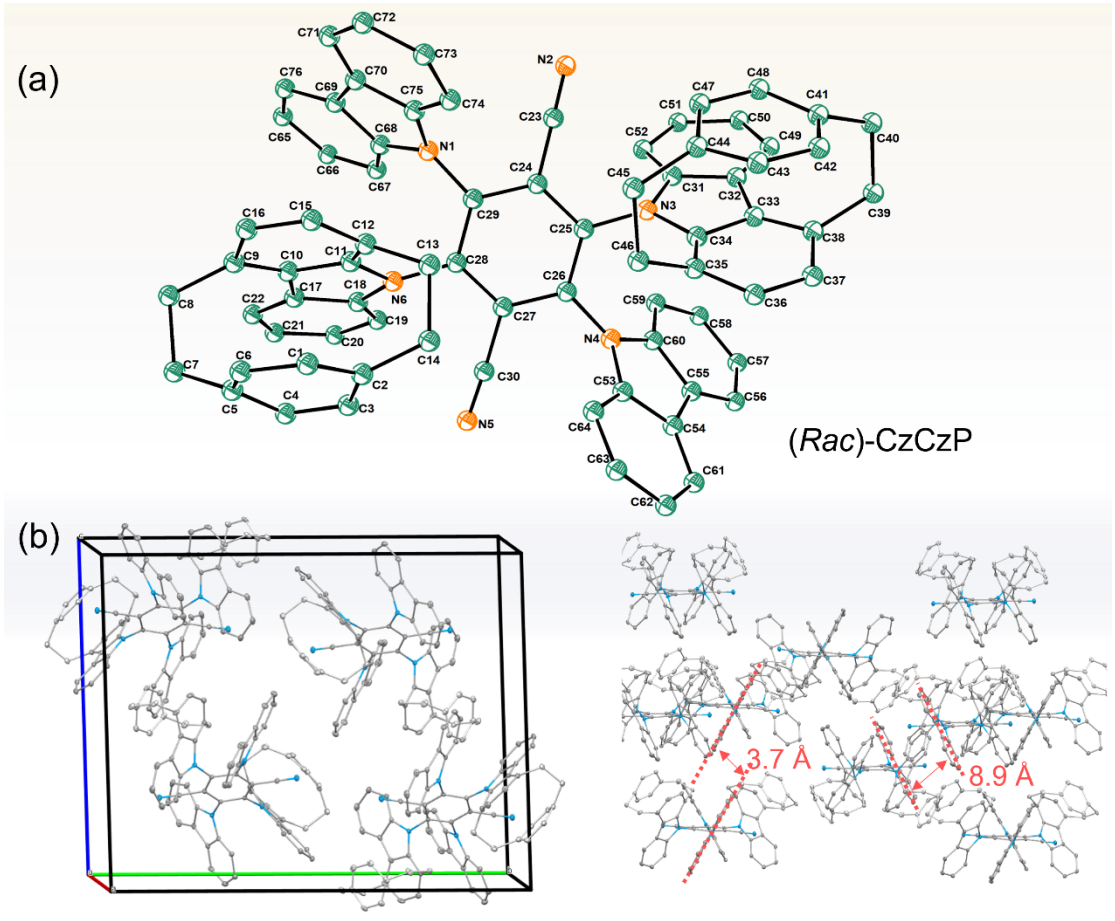

Fig. S19 (a) Representative ORTEP-style diagram[8] and (b) packing diagram of compound (*Rac*)-CzCzP. Thermal ellipsoids are set at 20% probability level. All the hydrogen atoms and solvents are omitted for clarity.

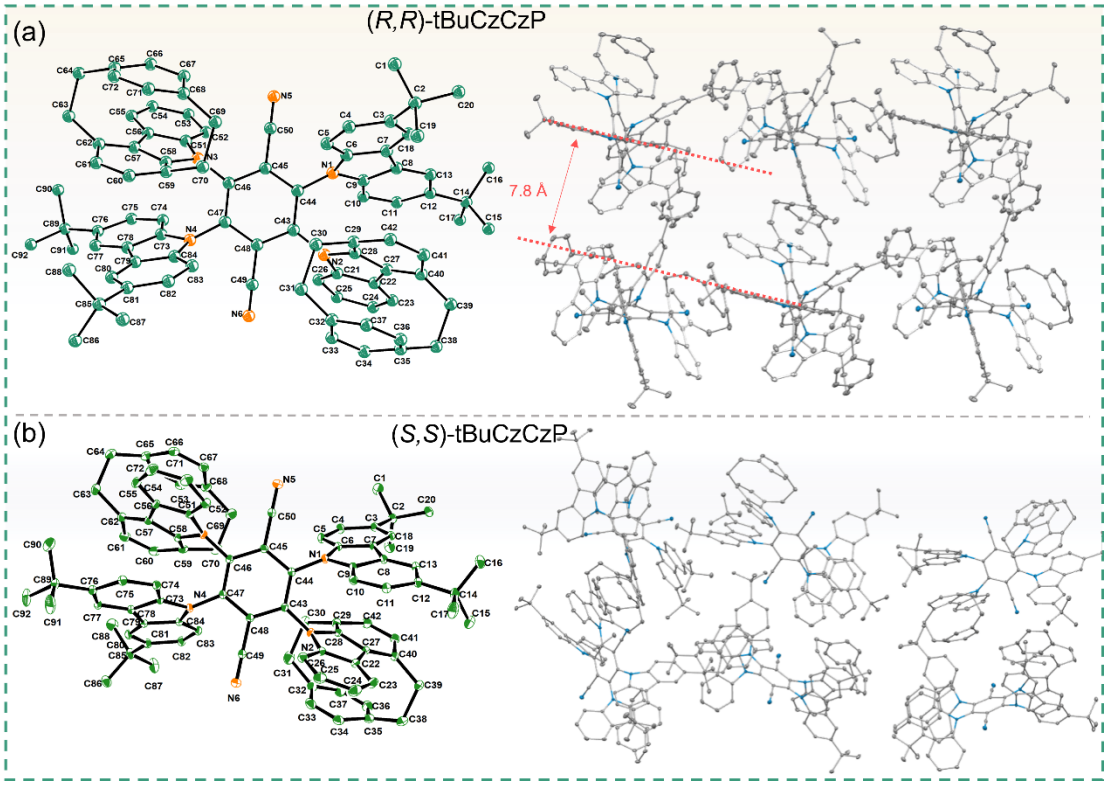

Fig. S20 Representative ORTEP-style diagram and packing diagram of compound (a) (*R,R*)-tBuCzCzP and (b) (*S,S*)-tBuCzCzP. Thermal ellipsoids are set at 20% probability level. All the hydrogen atoms and solvents are omitted for clarity.

Table S2. Crystallographic data for (*Rac*)-CzCzP , (*R,R*)-tBuCzCzP and (*S,S*)-tBuCzCzP

Identification code	**(*Rac*)-CzCzP**	**(*R,R*)-tBuCzCzP**	**(*S,S*)-tBuCzCzP**
CCDC number	2444969	2444965	2444968
Empirical formula	$C_{78}H_{56}Cl_4N_6$	$C_{93}H_{86}Cl_2N_6$	$C_{93}H_{86}Cl_2N_6$
Formula weight	1219.08	1358.57	1358.57
Temperature/K	193.00	223.00	223.00
Crystal system	monoclinic	tetragonal	tetragonal
Space group	$P2_1/c$	$P4_32_12$	$P4_12_12$
a/Å	13.5469(10)	15.8363(7)	15.8075(6)
b/Å	23.8140(14)	15.8363(7)	15.8075(6)
c/Å	19.6420(12)	58.867(4)	58.762(4)
α/°	90	90	90

Identification code	**(*Rac*)-CzCzP**	**(*R,R*)-tBuCzCzP**	**(*S,S*)-tBuCzCzP**
β/°	108.456(2)	90	90
γ/°	90	90	90
Volume/Å^3	6010.7(7)	14763.1(17)	14683.4(14)
Z	4	8	8
ρ_{calc}(g/cm^3)	1.347	1.222	1.229
μ/mm^{-1}	0.250	1.189	1.195
F(000)	2536.0	5760.0	5760.0
Crystal size/mm^3	0.14 × 0.13 × 0.1	0.13 × 0.11 × 0.08	0.12 × 0.1 × 0.09
Radiation (Å)	MoKα (λ= 0.71073)	CuKα (λ = 1.54178)	CuKα (λ = 1.54178)
2Θ range for data collection/°	3.602 to 50.764	5.778 to 152.946	5.79 to 149.368
Index ranges	-16 ≤ h ≤ 13, -28 ≤ k ≤ 28, -23 ≤ l ≤ 23	-18 ≤ h ≤ 19, -19 ≤ k ≤ 19, -71 ≤ l ≤ 73	-19 ≤ h ≤ 19, -19 ≤ k ≤ 19, -72 ≤ l ≤ 73
Reflections collected	46429	220544	291379
R_{int}	0.0594	0.0710	0.0627
Data/restraints/parameters	11012/718/1011	15188/88/950	15043/72/950
Goodness-offit on F^2	1.035	1.059	1.043
Final *R* indexes [I>2σ (I)]	R_1 = 0.0760, wR_2 = 0.1930	R_1 = 0.0411, wR_2 = 0.1049	R_1 = 0.0338, wR_2 = 0.0867
Final *R* indexes [all data]	R_1 = 0.1181, wR_2 = 0.2268	R_1 = 0.0474, wR_2 = 0.1093	R_1 = 0.0362, wR_2 = 0.0886
Largest diff. peak/hole /e Å^{-3}	0.93/-0.51	0.21/-0.25	0.22/-0.30
Flack parameter	\	0.019(5)	0.015(3)

$R_1 = \Sigma(||Fo| - |Fc||)/\Sigma|Fo|$; $wR_2 = \{\Sigma w(|Fo|^2 - |Fc|^2)^2/\Sigma w(|Fo|^2)^2\}^{1/2}$.

7. Theoretical calculation

Table S3. Cartesian coordinates of (*S*,*S*)-CzCzP at the optimized S_0 geometry.

Center Number	Atomic Number	Atomic Type	Coordinates (Angstroms) X	Y	Z
1	6	0	-0.344035	-1.24909	-1.21704
2	6	0	-0.960268	-0.78443	-0.03662
3	6	0	-0.958205	0.602564	0.239681
4	6	0	-0.367565	1.555103	-0.62515
5	6	0	0.258811	1.088582	-1.79925
6	6	0	0.264691	-0.29869	-2.0711
7	6	0	0.217359	4.223257	2.976516
8	6	0	-0.347369	5.479662	2.763382
9	6	0	0.461845	6.60605	2.557653
10	6	0	1.820432	6.48278	2.88205
11	6	0	2.387634	5.224236	3.088265
12	6	0	1.60999	4.061753	2.98299
13	6	0	0.565578	3.869975	-0.22685
14	6	0	0.027357	5.176312	-0.38246
15	6	0	0.861127	6.303716	-0.22309
16	6	0	2.234594	6.048113	-0.20004
17	6	0	2.735403	4.758747	0.009699
18	6	0	1.896457	3.652177	0.174803
19	6	0	2.230007	2.731433	2.613842
20	6	0	2.366845	2.487935	1.026513
21	6	0	0.369568	7.676517	0.19586
22	6	0	-0.058715	7.767235	1.736148
23	6	0	-1.694126	3.639706	-0.52245
24	6	0	-1.408549	5.024956	-0.54639
25	6	0	-2.464918	5.927146	-0.74243
26	6	0	-3.758508	5.442267	-0.9136
27	6	0	-4.014555	4.063313	-0.89954
28	6	0	-2.984872	3.143395	-0.70889
29	7	0	-0.489889	2.930539	-0.31764
30	6	0	2.600388	-4.30311	-2.80667
31	6	0	1.930495	-5.42072	-3.30166
32	6	0	1.966213	-6.64313	-2.61572
33	6	0	2.93319	-6.78182	-1.60988
34	6	0	3.597285	-5.66154	-1.10787
35	6	0	3.318219	-4.38004	-1.60488
36	6	0	0.083735	-3.71061	-0.84666
37	6	0	-0.525932	-4.89213	-1.34911
38	6	0	-0.160896	-6.14945	-0.82239
39	6	0	0.578518	-6.1224	0.363045

Center Number	Atomic Number	Atomic Type	Coordinates (Angstroms) X	Y	Z
40	6	0	1.214423	-4.95639	0.802936
41	6	0	1.120668	-3.74879	0.103892
42	6	0	3.530737	-3.14568	-0.75569
43	6	0	2.271391	-2.76173	0.173907
44	6	0	-0.268177	-7.45817	-1.58254
45	6	0	0.813358	-7.61628	-2.75179
46	6	0	-1.249663	-3.08868	-2.60235
47	6	0	-1.35087	-4.49431	-2.47756
48	6	0	-2.184439	-5.19086	-3.36543
49	6	0	-2.891607	-4.48834	-4.33707
50	6	0	-2.785527	-3.09304	-4.43196
51	6	0	-1.967013	-2.3738	-3.56271
52	7	0	-0.366588	-2.60745	-1.61075
53	6	0	-5.003981	-2.73699	-0.24982
54	6	0	-5.356678	-3.45008	0.907136
55	6	0	-4.477704	-3.53576	1.98321
56	6	0	-3.23127	-2.90521	1.895778
57	6	0	-2.887634	-2.20575	0.713583
58	6	0	-2.12141	-2.75898	2.816253
59	6	0	-1.142328	-1.97149	2.165663
60	7	0	-1.599577	-1.65967	0.871657
61	6	0	-1.884489	-3.21168	4.119287
62	6	0	-0.69179	-2.86875	4.749564
63	6	0	0.26479	-2.08	4.090137
64	6	0	0.055276	-1.62273	2.790064
65	6	0	-3.768181	-2.1018	-0.36267
66	6	0	4.601789	1.791664	-2.72568
67	6	0	4.821723	2.644355	-3.81962
68	6	0	3.750513	3.218582	-4.4981
69	6	0	2.446139	2.934971	-4.07703
70	6	0	2.245271	2.080354	-2.96729
71	6	0	1.135479	3.329614	-4.55366
72	6	0	0.181232	2.706231	-3.71357
73	7	0	0.863163	1.967401	-2.72819
74	6	0	0.696926	4.121509	-5.62106
75	6	0	-0.670298	4.268184	-5.8382
76	6	0	-1.600502	3.627903	-5.00367
77	6	0	-1.189922	2.835676	-3.9326
78	6	0	3.312911	1.499802	-2.28224
79	6	0	0.899268	-0.75589	-3.27231
80	7	0	1.418714	-1.12769	-4.24316
81	6	0	-1.599442	1.059829	1.437114

Center Number	Atomic Number	Atomic Type	Coordinates (Angstroms) X	Y	Z
82	7	0	-2.115451	1.430506	2.410252
83	1	0	-0.430196	3.351632	3.006651
84	1	0	-1.421783	5.556977	2.618454
85	1	0	2.469162	7.354518	2.830111
86	1	0	3.466886	5.140702	3.196029
87	1	0	2.926159	6.885577	-0.16271
88	1	0	3.796309	4.639908	0.214271
89	1	0	3.232306	2.648008	3.046464
90	1	0	1.635347	1.911795	3.029922
91	1	0	1.832938	1.567416	0.780373
92	1	0	3.422146	2.298942	0.808702
93	1	0	1.184317	8.387864	0.029237
94	1	0	-0.470546	8.025465	-0.41165
95	1	0	-1.151255	7.788146	1.794544
96	1	0	0.30009	8.729458	2.118191
97	1	0	-2.280376	6.995082	-0.77022
98	1	0	-4.57813	6.139024	-1.06045
99	1	0	-5.029675	3.701547	-1.03211
100	1	0	-3.196034	2.079796	-0.69578
101	1	0	2.452513	-3.34188	-3.29051
102	1	0	1.263944	-5.30189	-4.15194
103	1	0	3.063264	-7.7415	-1.11433
104	1	0	4.234351	-5.77108	-0.23293
105	1	0	0.816212	-7.06049	0.857519
106	1	0	1.933062	-5.03091	1.615098
107	1	0	4.394879	-3.28569	-0.09825
108	1	0	3.751972	-2.28261	-1.39208
109	1	0	1.953564	-1.75214	-0.0952
110	1	0	2.626145	-2.70738	1.207483
111	1	0	-0.114334	-8.27211	-0.86739
112	1	0	-1.261268	-7.6143	-2.01409
113	1	0	0.316488	-7.45282	-3.713
114	1	0	1.154717	-8.65745	-2.7416
115	1	0	-2.288507	-6.26763	-3.2955
116	1	0	-3.533211	-5.02611	-5.02843
117	1	0	-3.342285	-2.56054	-5.19707
118	1	0	-1.892056	-1.29534	-3.64916
119	1	0	-5.704535	-2.67702	-1.07727
120	1	0	-6.326735	-3.93437	0.963103
121	1	0	-4.756846	-4.07705	2.882407
122	1	0	-2.624671	-3.81904	4.631829
123	1	0	-0.498922	-3.20984	5.762006

Center Number	Atomic Number	Atomic Type	Coordinates (Angstroms) X	Y	Z
124	1	0	1.186585	-1.81766	4.600809
125	1	0	0.802173	-1.01786	2.288022
126	1	0	-3.505714	-1.5594	-1.26327
127	1	0	5.450341	1.347851	-2.21347
128	1	0	5.837775	2.853019	-4.14008
129	1	0	3.92282	3.874777	-5.34613
130	1	0	1.415071	4.607008	-6.2753
131	1	0	-1.022786	4.879134	-6.66355
132	1	0	-2.662891	3.750589	-5.19167
133	1	0	-1.917048	2.351414	-3.29095
134	1	0	3.152496	0.843855	-1.43388

Table S4. Cartesian coordinates of (*S*,*S*)-tBuCzCzP at the optimized S_0 geometry.

Center Number	Atomic Number	Atomic Type	Coordinates (Angstroms) X	Y	Z
1	6	0	-0.119366	-1.15261	-0.35569
2	6	0	0.253788	-0.24555	-1.37693
3	6	0	0.318725	1.133353	-1.06885
4	6	0	0.002873	1.670227	0.200998
5	6	0	-0.377167	0.774392	1.220942
6	6	0	-0.47251	-0.60774	0.906938
7	6	0	0.805728	4.908125	3.434006
8	6	0	0.257889	6.098652	2.959426
9	6	0	1.078226	7.179653	2.604258
10	6	0	2.412349	7.133107	3.031768
11	6	0	2.963289	5.936379	3.493625
12	6	0	2.195066	4.764151	3.552905
13	6	0	1.102686	3.966066	0.386107
14	6	0	0.697531	5.248623	-0.07523
15	6	0	1.600153	6.33357	-0.04405
16	6	0	2.943549	5.999221	0.13123
17	6	0	3.32567	4.735826	0.593221
18	6	0	2.393021	3.741332	0.903913
19	6	0	2.849864	3.401655	3.446131
20	6	0	2.721635	2.741059	1.992349
21	6	0	1.18411	7.786158	0.091263
22	6	0	0.615781	8.152839	1.538813
23	6	0	-1.086286	3.805824	-0.25867
24	6	0	-0.69938	5.151405	-0.44896
25	6	0	-1.619923	6.051111	-1.00798
26	6	0	-2.873545	5.593331	-1.40204

Center Number	Atomic Number	Atomic Type	Coordinates (Angstroms) X	Y	Z
27	6	0	-3.212976	4.239016	-1.26889
28	6	0	-2.320588	3.328695	-0.70535
29	7	0	-0.026651	3.092361	0.345267
30	6	0	2.650893	-4.83142	-1.38398
31	6	0	1.835489	-5.94162	-1.59159
32	6	0	1.816228	-7.0036	-0.67622
33	6	0	2.856035	-7.05399	0.262432
34	6	0	3.668034	-5.93814	0.475917
35	6	0	3.468917	-4.75323	-0.24801
36	6	0	0.300589	-3.51259	0.391167
37	6	0	-0.435488	-4.71955	0.267266
38	6	0	-0.097001	-5.84524	1.049183
39	6	0	0.761972	-5.60081	2.122231
40	6	0	1.512107	-4.42432	2.200782
41	6	0	1.429426	-3.42151	1.230438
42	6	0	3.874567	-3.41173	0.332159
43	6	0	2.657536	-2.57542	0.956364
44	6	0	-0.377019	-7.2852	0.660966
45	6	0	0.554259	-7.8261	-0.51986
46	6	0	-1.28535	-3.17765	-1.22949
47	6	0	-1.409978	-4.51538	-0.7867
48	6	0	-2.412387	-5.32795	-1.33712
49	6	0	-3.282096	-4.7965	-2.28394
50	6	0	-3.17274	-3.45457	-2.67259
51	6	0	-2.181903	-2.62974	-2.14343
52	7	0	-0.204077	-2.55988	-0.54816
53	6	0	-2.240578	0.518048	-5.03434
54	6	0	-1.671018	0.115563	-6.25898
55	6	0	-0.405048	-0.48407	-6.2252
56	6	0	0.259837	-0.68113	-5.01291
57	6	0	-0.356583	-0.2932	-3.8023
58	6	0	1.57386	-1.19095	-4.67383
59	6	0	1.703276	-1.10334	-3.27052
60	7	0	0.494658	-0.6269	-2.72416
61	6	0	2.649325	-1.63624	-5.45195
62	6	0	3.868847	-1.96493	-4.85451
63	6	0	3.977211	-1.81274	-3.45366
64	6	0	2.919879	-1.38637	-2.65367
65	6	0	-1.60382	0.326422	-3.80684
66	6	0	1.927817	-0.31433	4.893298
67	6	0	1.363807	0.091148	6.120076
68	6	0	0.166242	0.817086	6.07937

Center Number	Atomic Number	Atomic Type	Coordinates (Angstroms) X	Y	Z
69	6	0	-0.442599	1.121579	4.859654
70	6	0	0.156642	0.706602	3.650274
71	6	0	-1.666167	1.813687	4.509722
72	6	0	-1.767119	1.801453	3.10097
73	7	0	-0.626105	1.162721	2.562683
74	6	0	-2.676144	2.395316	5.286261
75	6	0	-3.804226	2.951566	4.679862
76	6	0	-3.887893	2.889638	3.27045
77	6	0	-2.897601	2.321663	2.474916
78	6	0	1.345194	-0.01757	3.659937
79	6	0	5.086198	-2.46033	-5.6592
80	6	0	4.789451	-2.55329	-7.16724
81	6	0	6.271069	-1.4861	-5.46197
82	6	0	5.493651	-3.86684	-5.16143
83	6	0	-2.381281	0.324891	-7.61186
84	6	0	-3.748378	1.016484	-7.45622
85	6	0	-1.500486	1.205445	-8.52861
86	6	0	-2.610717	-1.04589	-8.29028
87	6	0	2.010258	-0.23932	7.480621
88	6	0	3.325253	-1.02646	7.33059
89	6	0	2.320119	1.072996	8.237898
90	6	0	1.031994	-1.09311	8.320873
91	6	0	-4.945208	3.607134	5.481576
92	6	0	-4.680471	3.583067	6.998213
93	6	0	-5.101656	5.082628	5.044661
94	6	0	-6.268112	2.852529	5.212387
95	6	0	-1.088693	-1.45367	1.888378
96	7	0	-1.653892	-2.09506	2.675848
97	6	0	0.759823	2.031904	-2.09782
98	7	0	1.137861	2.75548	-2.92447
99	1	0	0.158055	4.046396	3.566521
100	1	0	-0.803649	6.132997	2.727229
101	1	0	3.065998	7.98559	2.859237
102	1	0	4.035	5.882863	3.672984
103	1	0	3.695483	6.781732	0.074934
104	1	0	4.36043	4.583923	0.890781
105	1	0	3.913944	3.498707	3.685042
106	1	0	2.42783	2.689192	4.161749
107	1	0	1.955126	1.971044	2.041067
108	1	0	3.666556	2.229273	1.777289
109	1	0	2.067996	8.404809	-0.09298
110	1	0	0.438746	8.086666	-0.65139

Center Number	Atomic Number	Atomic Type	Coordinates (Angstroms) X	Y	Z
111	1	0	-0.477965	8.146826	1.497718
112	1	0	0.922367	9.18202	1.758179
113	1	0	-1.353721	7.091435	-1.15768
114	1	0	-3.586736	6.28613	-1.83811
115	1	0	-4.181109	3.888425	-1.61381
116	1	0	-2.581294	2.278394	-0.63544
117	1	0	2.539785	-3.96734	-2.03105
118	1	0	1.101208	-5.91306	-2.39274
119	1	0	2.936764	-7.9045	0.936
120	1	0	4.367151	-5.94541	1.309426
121	1	0	0.985024	-6.40735	2.815296
122	1	0	2.307852	-4.36513	2.939136
123	1	0	4.612875	-3.57552	1.123481
124	1	0	4.357465	-2.7782	-0.41925
125	1	0	2.413173	-1.75333	0.282219
126	1	0	3.02248	-2.1193	1.882661
127	1	0	-0.196677	-7.90652	1.543634
128	1	0	-1.419822	-7.45329	0.376417
129	1	0	-0.012746	-7.7966	-1.45553
130	1	0	0.771015	-8.87942	-0.30912
131	1	0	-2.524161	-6.35765	-1.01766
132	1	0	-4.058451	-5.42192	-2.71418
133	1	0	-3.86636	-3.04247	-3.39934
134	1	0	-2.122438	-1.59783	-2.45317
135	1	0	-3.207314	1.006742	-5.02471
136	1	0	0.079475	-0.79033	-7.14736
137	1	0	2.524685	-1.70005	-6.52661
138	1	0	4.923964	-2.02932	-2.96905
139	1	0	3.057435	-1.25561	-1.58823
140	1	0	-2.074068	0.674411	-2.89312
141	1	0	2.850336	-0.88244	4.887611
142	1	0	-0.305881	1.145852	7.000108
143	1	0	-2.569723	2.393942	6.36473
144	1	0	-4.760972	3.297291	2.770609
145	1	0	-3.019125	2.294341	1.402942
146	1	0	1.816931	-0.35047	2.743154
147	1	0	5.677995	-2.91316	-7.6965
148	1	0	3.97469	-3.25303	-7.38188
149	1	0	4.526136	-1.57967	-7.59412
150	1	0	7.145232	-1.82767	-6.02834
151	1	0	6.56873	-1.40963	-4.41166
152	1	0	6.015408	-0.47939	-5.80952

Center Number	Atomic Number	Atomic Type	Coordinates (Angstroms) X	Y	Z
153	1	0	4.678171	-4.58498	-5.29856
154	1	0	6.363935	-4.2329	-5.71849
155	1	0	5.7573	-3.86526	-4.09938
156	1	0	-4.212359	1.140645	-8.44034
157	1	0	-4.438584	0.428731	-6.84156
158	1	0	-3.655741	2.012415	-7.01028
159	1	0	-1.99185	1.361996	-9.49598
160	1	0	-0.526559	0.746302	-8.72366
161	1	0	-1.320625	2.186979	-8.07741
162	1	0	-3.239272	-1.69321	-7.66912
163	1	0	-3.111021	-0.91616	-9.25704
164	1	0	-1.669649	-1.57382	-8.47327
165	1	0	3.746599	-1.23136	8.320352
166	1	0	3.172041	-1.99088	6.834748
167	1	0	4.077072	-0.4657	6.764799
168	1	0	2.775933	0.855411	9.210795
169	1	0	1.416616	1.662483	8.421095
170	1	0	3.016771	1.700572	7.671533
171	1	0	0.088606	-0.56994	8.50492
172	1	0	0.795553	-2.03471	7.813987
173	1	0	1.473142	-1.33399	9.295105
174	1	0	-5.511769	4.06262	7.525611
175	1	0	-4.594664	2.561309	7.383121
176	1	0	-3.767243	4.12653	7.263101
177	1	0	-5.912536	5.563368	5.604205
178	1	0	-5.337183	5.172004	3.979688
179	1	0	-4.181976	5.647766	5.230442
180	1	0	-6.192487	1.803708	5.518816
181	1	0	-7.090741	3.31041	5.773941
182	1	0	-6.541935	2.870131	4.153015

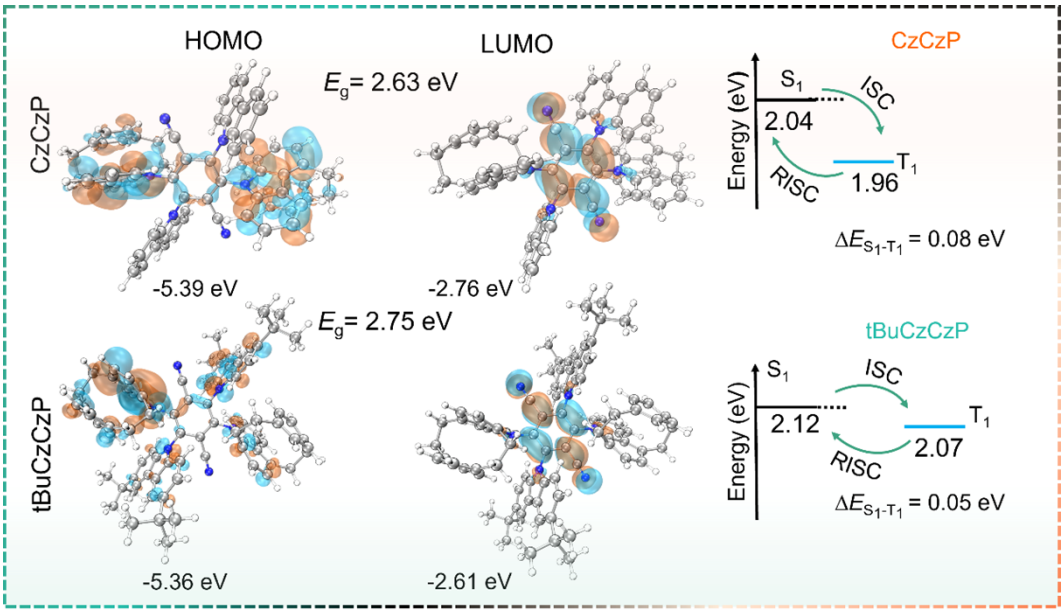

Fig. S21 Ground-state optimized HOMO/LUMO distributions, energy level alignments (ΔE_{ST}) for CzCzP and tBuCzCzP.

Table S5. TD-DFT calculation results for the three emitters in the optimized S_0 geometries

Emitter	State	*E* [eV]	λ [nm]	*f*	Main contribution [%]	
CzCzP	S_1	2.0433	606.8	0.0518	H→L	98.78276
	S_2	2.138	579.91	0.0003	H-1→L	96.5911
	S_3	2.1822	568.16	0.0088	H-4→L	13.48466
					H-2→L	85.73951
	S_4	2.2278	556.52	0.0003	H-5→L	7.137398
					H-3→ L	91.35194
	S_5	2.3379	530.32	0.0233	H-4→L	85.60861
					H-2→L	13.63778
	S_6	2.3801	520.93	0.0007	H-5→L	88.67124
					H-3→L	6.728579
	S_7	2.5516	485.91	0.0014	H-8→L	61.28352
					H-7→ L	6.154435
					H-6→L	32.1955
	S_8	2.5563	485.01	0.0002	H-9→L	58.83087
					H-7→L	36.25261
					H-6→L	4.104113
tBuCzCzP	S_1	2.1242	583.66	0.0218	H→L	97.21478
	S_2	2.159	574.25	0.0171	H-1→L	97.63913
	S_3	2.2868	542.18	0.0014	H-5→L	11.09488
					H-3→L	11.24992
					H-2→L	75.54909
	S_4	2.306	537.65	0.0114	H-5→ L	4.154115

Emitter	State	*E* [eV]	λ [nm]	*f*	Main contribution [%]	
					H-4→L	55.61328
					H-3→L	30.08087
					H-2→L	8.877212
	S_5	2.319	534.64	0.0071	H-5→L	2.032934
					H-1→L	42.33104
					H-3→ L	45.32091
					H-2→L	8.600463
	S_6	2.3575	525.91	0.0004	H-5→L	81.23026
					H-3→L	12.60321
					H-3→L	4.127639
	S_7	2.5847	479.69	0.0005	H-7→L	2.438074
					H-6→L	97.05031
	S_8	2.5875	479.16	0.0003	H-7→ L	96.88042
					H-6→ L	2.42969

8. Photophysical and chiral property

Table S6. Photophysical properties of CzCzP and tBuCzCzP.

Compound	λ_{abs} [a]	λ_{PL} [a]	Stokes Shift [a]	FWHM [a]	ΔE_{ST} [b]	Φ_{PL} [c]	Φ_{PL} [d]	τ_P [e]	τ_d [e]	k_{RISC} [f]
	[nm]	[nm]	[nm]	[nm]	[eV]	(%)	(%)	(ns)	(μs)	(10^5 s^{-1})
CzCzP	474	584	111	92	–0.01	61.5	81.1	1.85	1.38	7.4
tBuCzCzP	487	580	93	83	–0.04	68.2	87.0	1.63	1.28	8.1

a) Maximum wavelength of UV-absorption (λ_{abs}), photoluminescence peak (λ_{PL}), Stokes Shift and full-width at half-maximum (FWHM) of the PL spectrum. b) S_1-T_1 energy gap (ΔE_{ST}); Absolute photoluminescence efficiency in c) toluene solution and d) neat films, e) the lifetime of prompt (τ_p) and delayed (τ_d) components of neat film at room temperature. f) reverse intersystem crossing (k_{RISC}) rate.

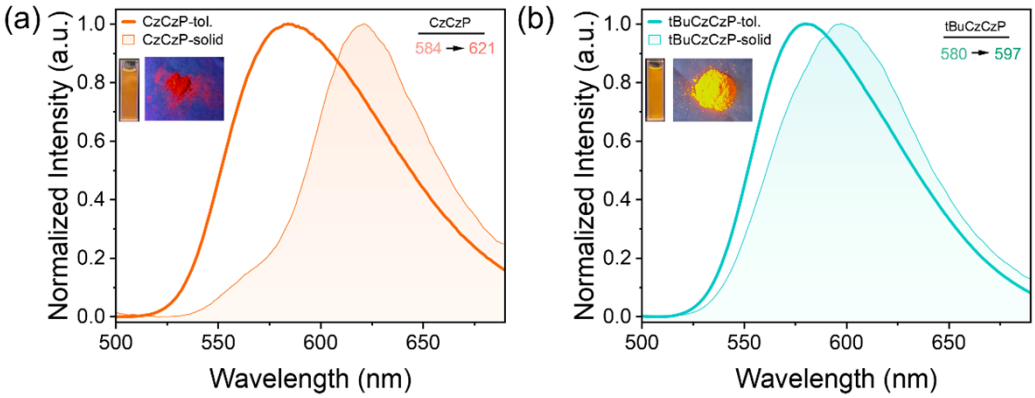

Fig. S22 PL spectra of (a) CzCzP and (b) tBuCzCzP in toluene and at solid state (r.t, λex = 356 and 360 nm).

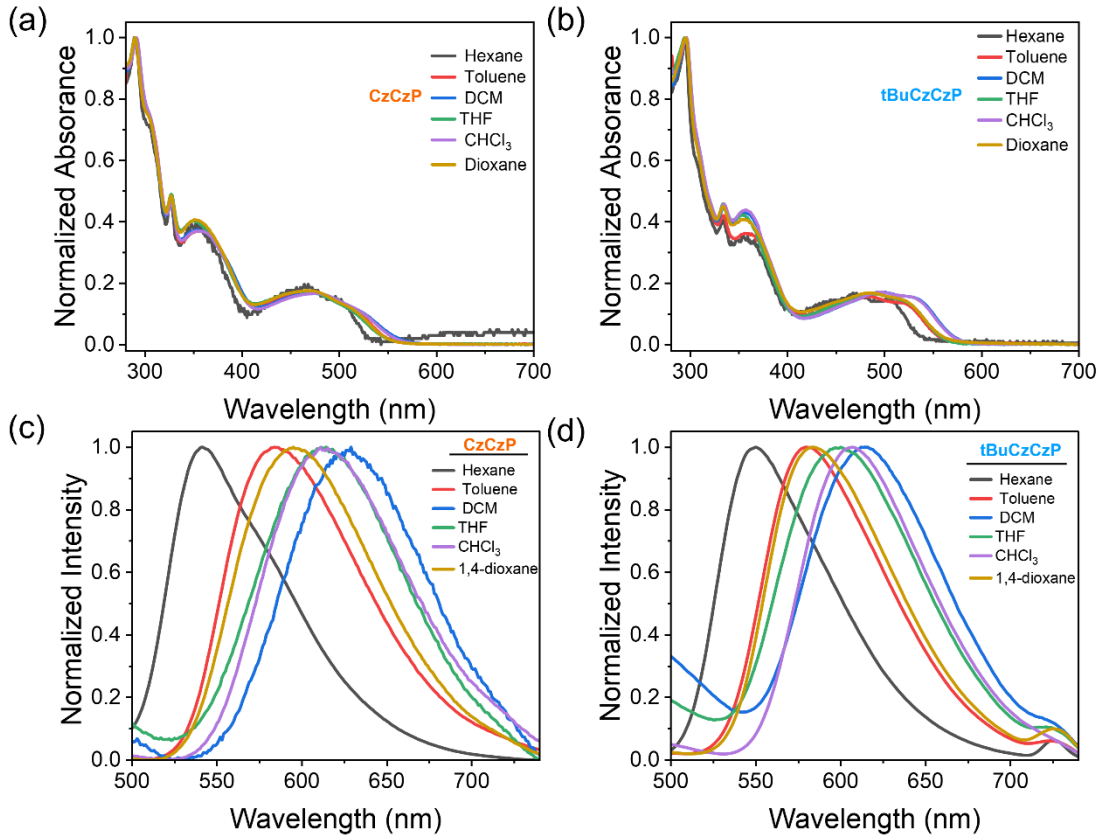

Fig. S23 Normalized absorbance (a, b) and PL (c, d) spectra of CzCzP and tBuCzCzP in various solvents (1×10^{-5} M, 298 K, excited by 356 and 360 nm).

Table S7. Photophysical data of CzCzP and tBuCzCzP in different solvents.

Compound	Solvent	λ_{abs} (max/nm)	λ_{PL} (max/nm)	Stokes shift (nm)	FWHM (nm)
CzCzP	Hexane	467	541	74	78
	Toluene	473	584	111	92
	DCM	475	629	154	96
	THF	470	614	144	99
	$CHCl_3$	478	611	133	98
	1,4-Dioxane	464	595	131	96
tBuCzCzP	Hexane	468	550	82	77
	Toluene	487	580	93	83
	DCM	498	614	116	93
	THF	488	600	112	97
	$CHCl_3$	495	607	112	86
	1,4-Dioxane	487	584	97	85

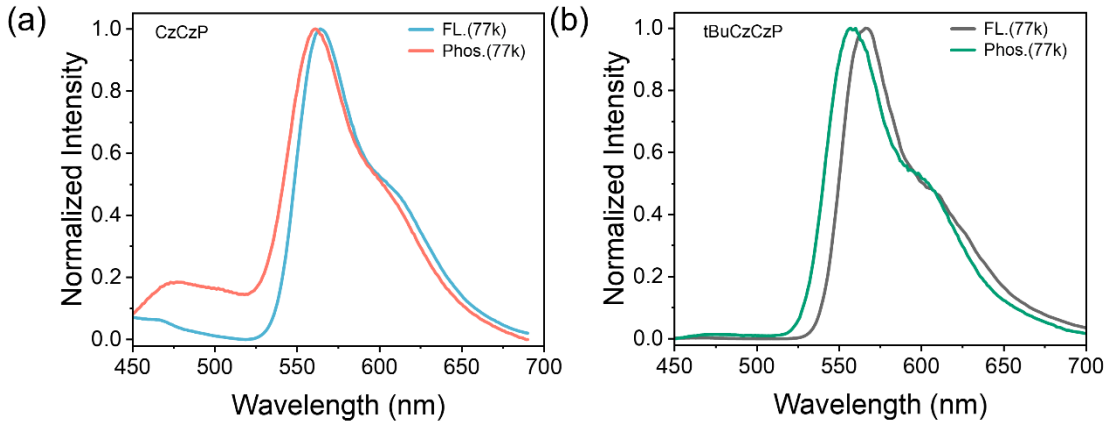

Fig. S24 Low-temperature fluorescence and phosphorescence spectra at 77 K of CzCzP and tBuCzCzP in toluene.

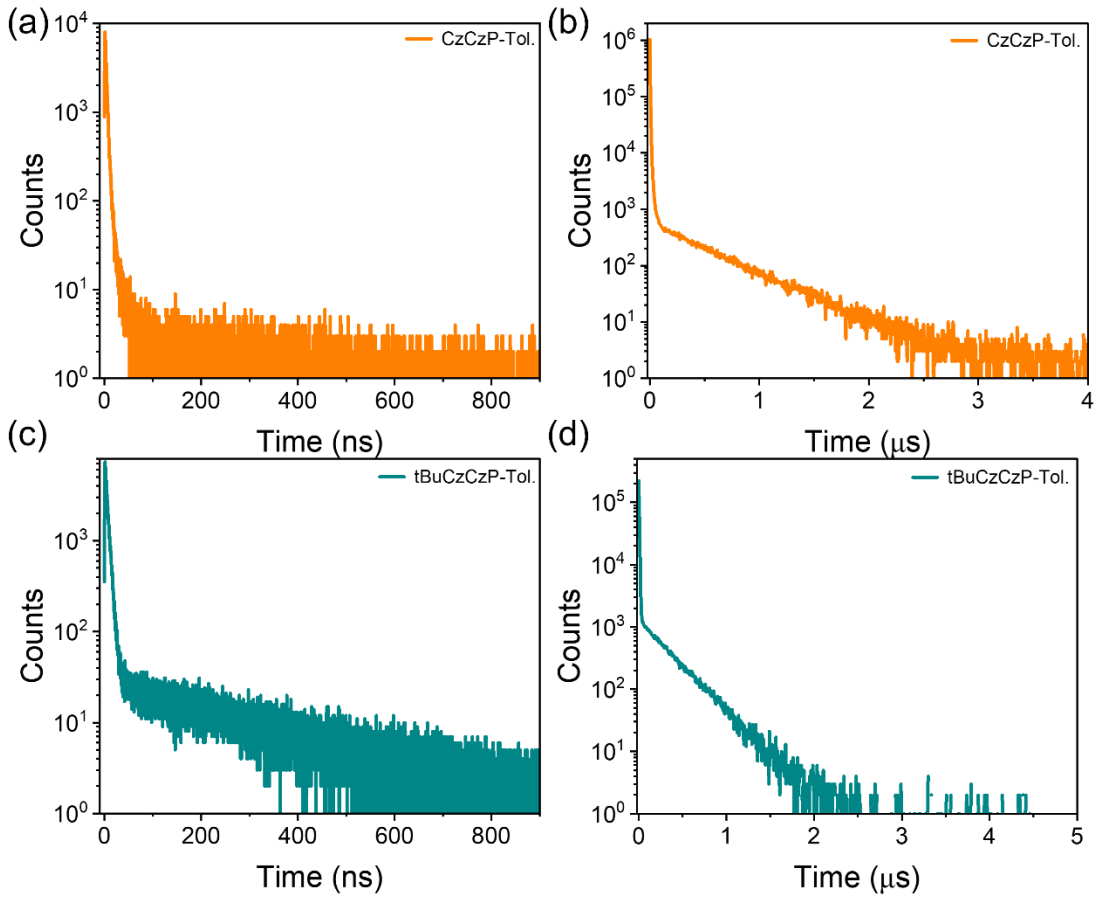

Fig. S25 Transient photoluminescence decay curves of CzCzP and tBuCzCzP in toluene; a) and c) prompt fluorescence (PF) decay curves at nanosecond scale, c) and d) delayed fluorescence (DF) curves at microsecond scale.

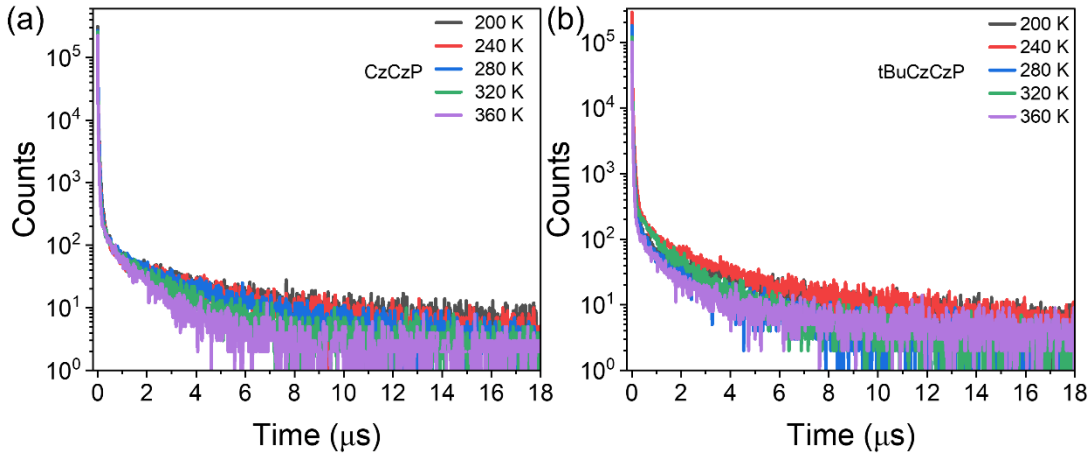

Fig. S26 Temperature dependent transient PL decay curves of the doped films of a) CzCzP and b) tBuCzCzP

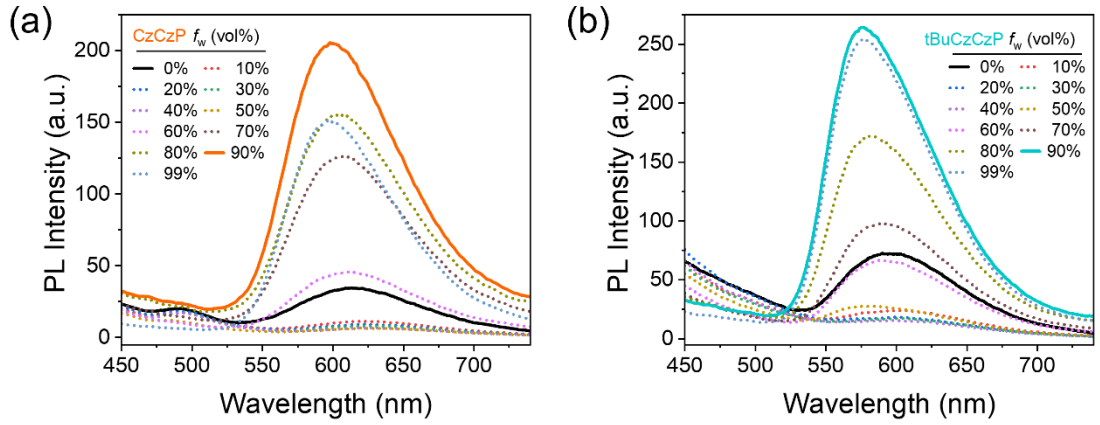

Fig. S27 PL spectra of CzCzP and tBuCzCzP in 1,4-Dioxane/H_2O mixtures with different water fractions (f_w) (1.0×10^{-5} mol L^{-1} λ_{ex} = 356 and 360 nm).

9. Chiroptical property

Table S8. Calculated $|\mu_e|$, $|\mu_m|$, and $\vartheta_{e,m}$ values, the absorption dissymmetry factor $g_{abs,\ calcd.}$ and the experimental $g_{abs.}$

Compound	$\lvert\mu_e\rvert \times 10^{-18}$ (esu cm)	$\lvert\mu_m\rvert \times 10^{-22}$ (erg G^{-1})	$\vartheta_{e,m}$ (°)	$\lvert g_{abs,\ calcd.}\rvert$ $\times 10^{-4}$	g_{abs} [a] $\times 10^{-3}$
(S,S)-CzCzP	2.59	8.98	77.8	2.93	–1.5/1.6
(S,S)-tBuCzCzP	1.64	11	93.7	1.7	–1.0/1.1

a) Absorption dissymmetry factor g_{abs} is calculated using the equation (g_{abs} =CD/(32980 × absorbance)), where the CD (in mdeg) and the absorbance can be obtained from CD spectral measurement.[9]

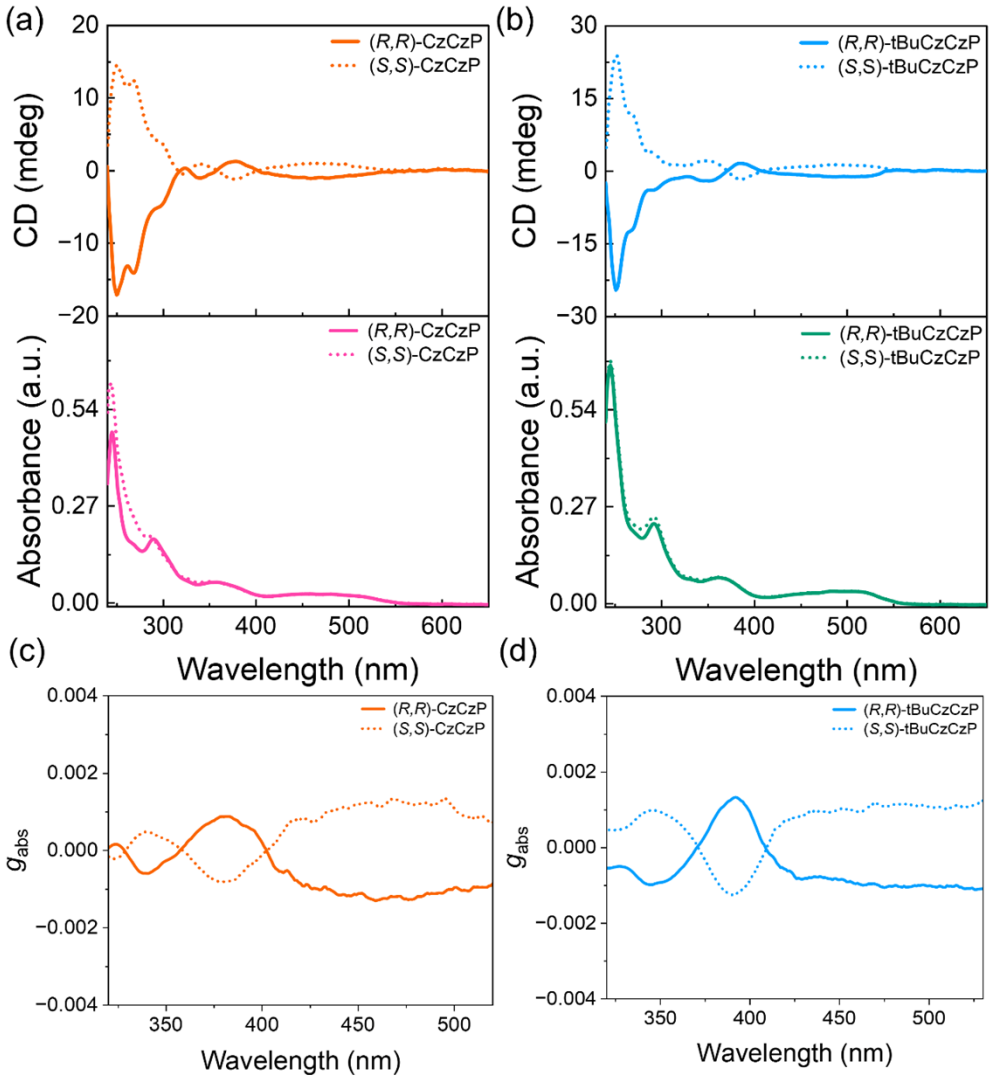

Fig. S28 CD spectra and corresponding absorption spectra of (a) (*R,R)/(S,S*)-CzCzP and (b) (*R,R)/(S,S*)-tBuCzCzP in toluene. The g_{abs} versus wavelength curves of (c) (*R,R)/(S,S*)-CzCzP and (d) (*R,R)/(S,S*)-tBuCzCzP.

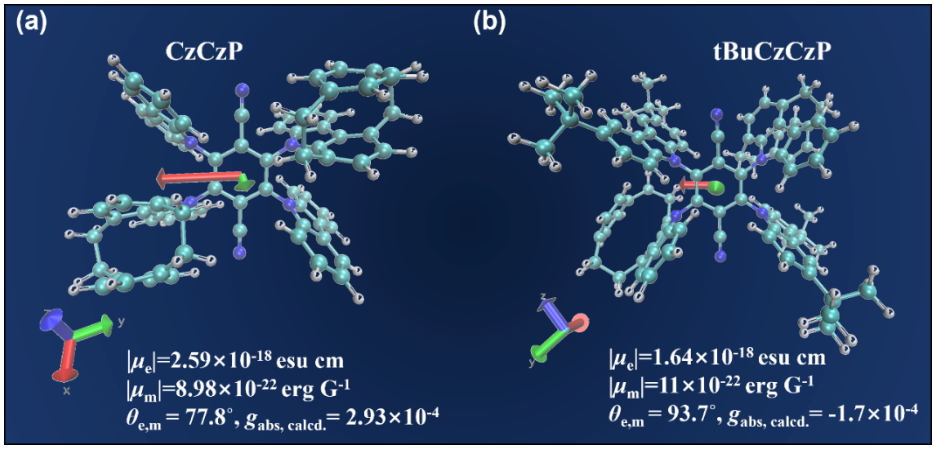

Fig. S29 Calculated μ_e (red arrow), μ_m (green arrow), and $\vartheta_{e,m}$ values of the S_1 state of CzCzP and tBuCzCzP.

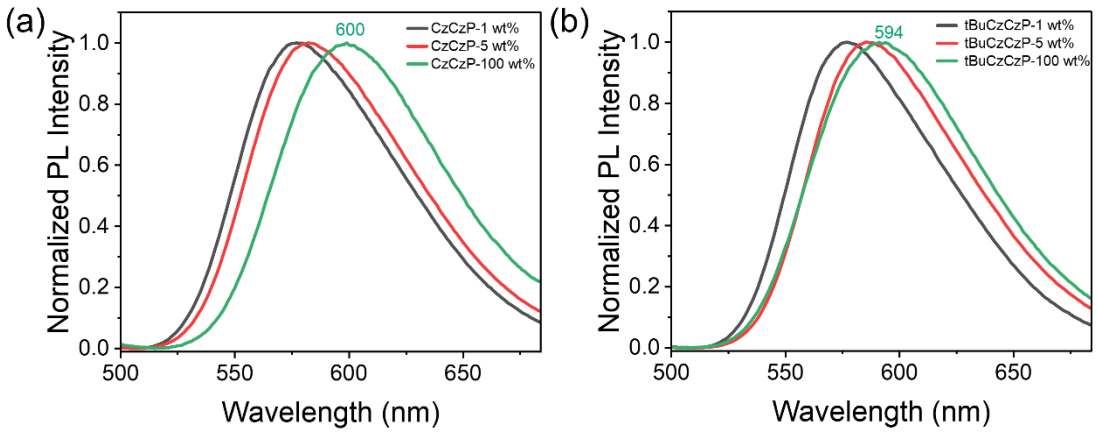

Fig. S30 Normalized photoluminescence spectra of (a) (*S, S*)-CzCzP and (b) (*S, S*)tBuCzCzP films at various doping concentrations (1 wt%, 5 wt%, and neat films), excited at 356 and 360 nm, respectively.

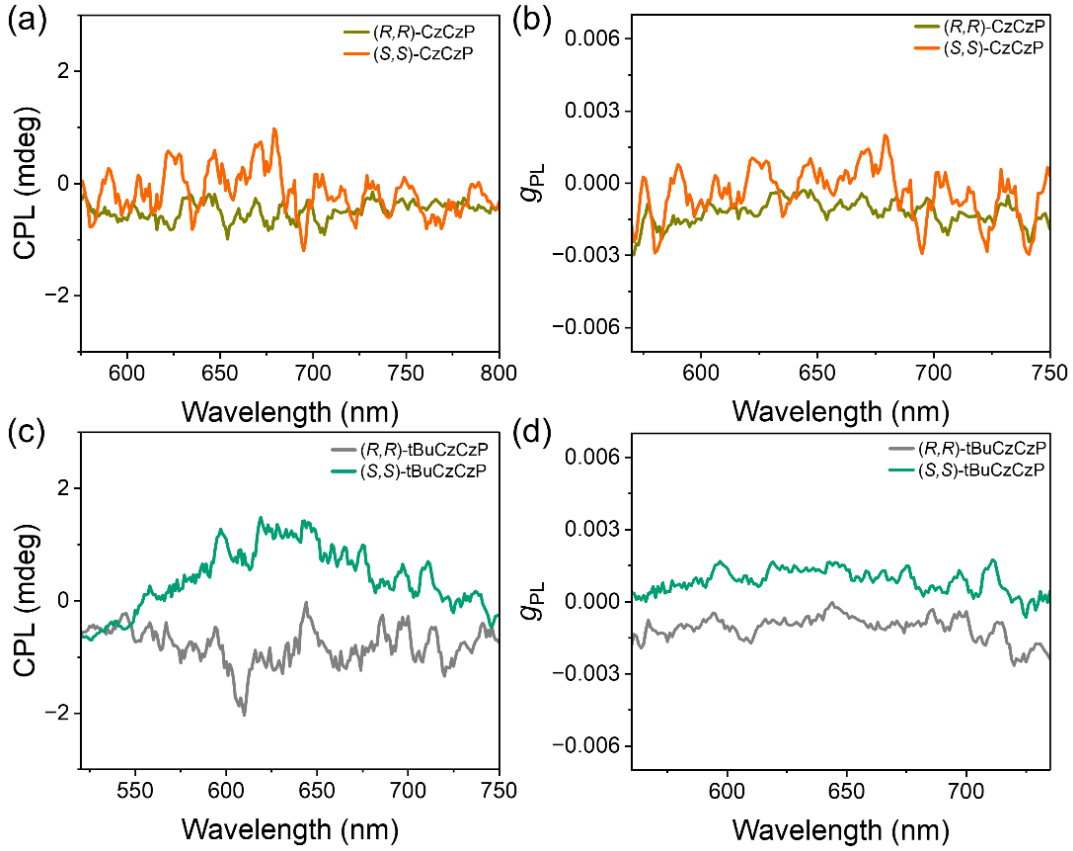

Fig. S31 (a) CPL spectra and (b) g_{PL} value of the neat films of (*R,R*)/(*S,S*)-CzCzP; (c) CPL spectra and (d) g_{PL} value of the neat films of (*R,R*)/(*S,S*)-tBuCzCzP.

10. Device fabrication and EL characteristics

CP-OLEDs were fabricated with the following structure: ITO (indium tin oxide)/ HATCN (1,4,5,8,9,11-hexaazatriphenyl-hexacarbonitrile, 5 nm)/ TAPC (di-[4-(N,N-

dihydroxy-amino)[4-(N,N-dihydroxy-amino)phenyl]cyclohexane, 30 nm)/ mCP (1,3-bis(N-carbazolyl)benzene, 10 nm)/ 2,6-DCzPPy (2,6-bis(3-(9H-carbazol-9-yl)phenyl)pyridine) : emitter (20 nm)/ TmPyPb (1,3,5-tris(meso-pyridin-3-ylphenyl)benzene, 40 nm)/ LiF (1 nm)/ Al (100 nm).

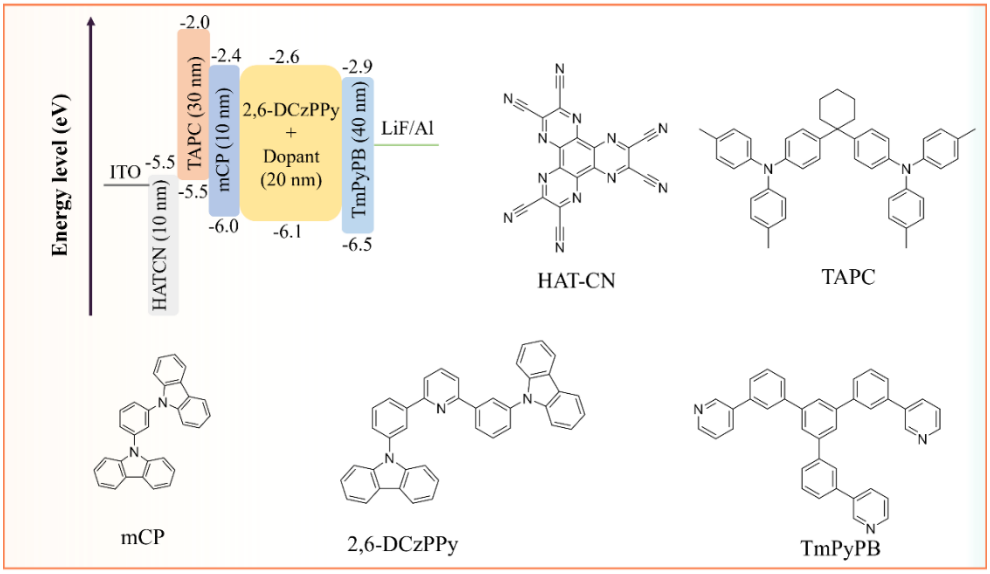

Fig. S32 Multilayer device architecture with energy level alignment and chemical structures of key materials.

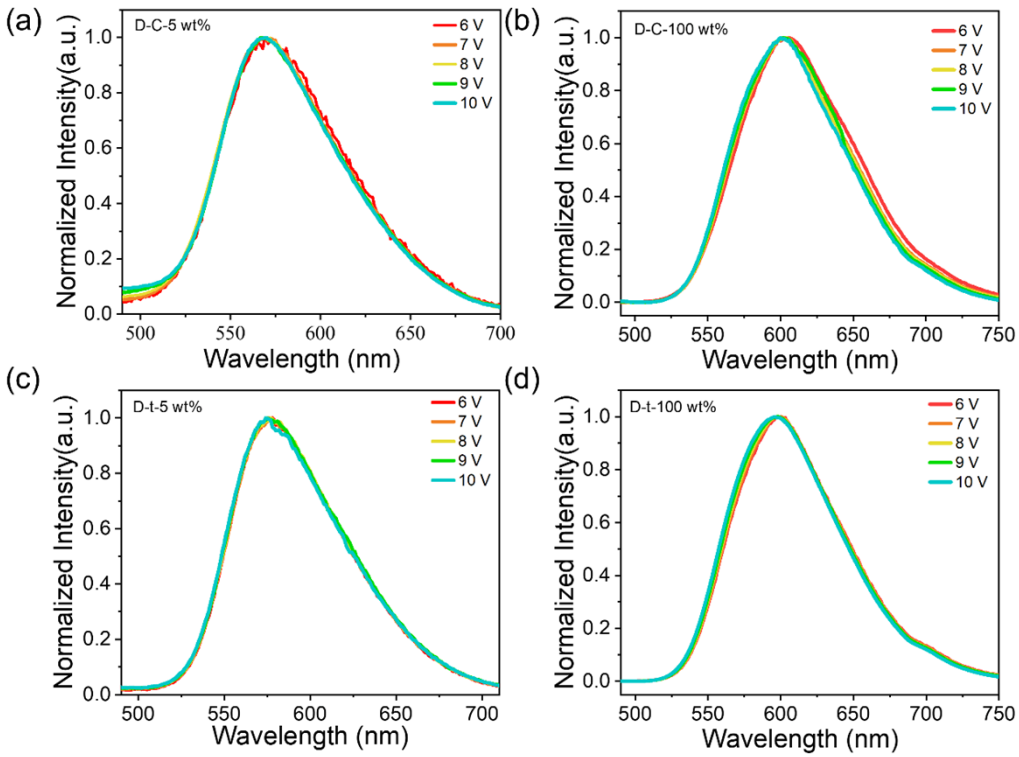

Fig. S33 EL spectra of (a) D-C-5 wt%, (b) D-C-100 wt%, (c) D-t-5wt%, (d) D-t-100 wt% taken at various voltages from 6 to 10 V.

Table S9. EL performance data of 5 wt% doped and non-doped OLEDs.

Device	λ_{EL} [a] (nm)	FWHM (nm)	CIE (x, y)	V_{on} [b] (V)	L_{max} [c] (cd m^{-2})	CE_{max} [c] (cd A^{-1})	PE_{max} [c] (lm W^{-1})	EQE [d] (%)
D-C-5 wt%	568	78	(0.48, 0.51)	4.7	35930	30.64	11.61	10.6/6.8
D-t-5 wt%	577	76	(0.52, 0.48)	5	36306	36.25	12.25	13.4/10.9
D-C-100 wt%	602	90	(0.57, 0.43)	4	35516	15.92	10.75	8.1/5.3
D-t-100 wt%	598	88	(0.56, 0.44)	3.8	37133	18.06	9.78	8.8/7.6

a) Electroluminescence peak at 7 V; b) Turn on voltage; c) The maximum luminescence (L_{max}), current efficiency (CE_{max}) and power efficiency (PE_{max}); d) The external quantum efficiency: maximum, values at 20,000 cd m^{-2}.

11. References

1. P. Jiang, J. Miao, X. Cao, H. Xia, K. Pan, T. Hua, X. Lv, Z. Huang, Y. Zou and C. Yang, *Adv. Mater.*, 2022, **34**, e2106954.
2. M. J. Frisch, G. W. Trucks, H. B. Schlegel, G. E. Scuseria, M. A. Robb, J. R. Cheeseman, G. Scalmani, V. Barone, B. Mennucci, G. A. Petersson, H. Nakatsuji, M. Caricato, X. Li, H. P. Hratchian, A. F. Izmaylov, J. Bloino, G. Zheng, J. L. Sonnenberg, M. Hada, M. Ehara, K. Toyota, R. Fukuda, J. Hasegawa, M. Ishida, T. Nakajima, Y. Honda, O. Kitao, H. Nakai, T. Vreven, J. A. Montgomery Jr., J. E. Peralta, F. Ogliaro, M. J. Bearpark, J. Heyd, E. N. Brothers, K. N. Kudin, V. N. Staroverov, R. Kobayashi, J. Normand, K. Raghavachari, A. P. Rendell, J. C. Burant, S. S. Iyengar, J. Tomasi, M. Cossi, N. Rega, N. J. Millam, M. Klene, J. E. Knox, J. B. Cross, V. Bakken, C. Adamo, J. Jaramillo, R. Gomperts, R. E. Stratmann, O. Yazyev, A. J. Austin, R. Cammi, C. Pomelli, J. W. Ochterski, R. L. Martin, K. Morokuma, V. G. Zakrzewski, G. A. Voth, P. Salvador, J. J. Dannenberg, S. Dapprich, A. D. Daniels, Ö. Farkas; J. B. Foresman, J. V. Ortiz, J. Cioslowski and D. J. Fox, Gaussian 09, Revision D.01, Gaussian, Inc.: Wallingford, CT, 2009.
3. T. Lu and F. Chen, *J. Comput. Chem.*, 2012, **33**, 580-592.
4. W. Humphrey, A. Dalke and K. Schulten, *J. Mol. Graph.*, 1996, **14**, 33-38, 27-38.
5. D. J. Shin, S. C. Kim and J. Y. Lee, *J. Mater. Chem. C*, 2022, **10**, 4821-4830.
6. N. Sharma, E. Spuling, C. M. Mattern, W. Li, O. Fuhr, Y. Tsuchiya, C. Adachi, S. Brase, I. D. W. Samuel and E. Zysman-Colman, *Chem. Sci.*, 2019, **10**, 6689-6696.
7. W. L. Zhao, K. K. Tan, W. C. Guo, C. H. Guo, M. Li and C. F. Chen, *Adv. Sci.* , 2024, **11**, e2309031.
8. L. J. Farrugia, *J. Appl. Cryst.*, 2012, **45**, 849-854.
9. Y. Liu, Y. Wei, Z. Luo, B. Xu, M. He, P. Hong, C. Li and Z. Quan, *Chem. Sci.*, 2024, **15**, 15480-15488.